HARDI reconstruction challenge 2013

Sunday April 7th, 2013

Westin San Francisco Market Street
San Francisco, CA, USA

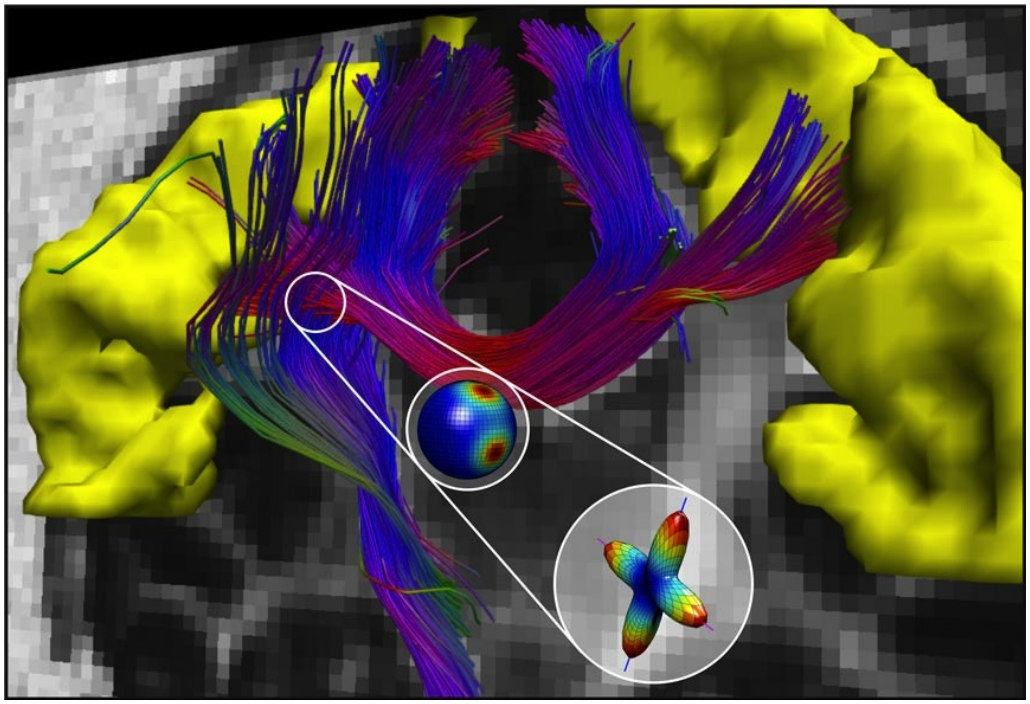

Abstract

Validation is the bottleneck for the diffusion magnetic resonance imaging (MRI) community.

Diffusion MRI is a powerful imaging modality which is sensitive to the random movement of the water molecules in biological tissues. By studying the anisotropy of this diffusion process in white matter it is possible to highlight structures otherwise invisible with other imaging modalities and to infer the neuronal wiring of the brain. The study of this connectivity is of major importance in a clinical perspective, with particular emphasis on neurological disorders which, nowadays, affect up to one billion people worldwide.

In the last few years a *multitude of new reconstruction approaches* have been proposed to recover the local intra-voxel fiber structure. Some of them aim at improving the quality of the reconstructions while others focus on reducing the acquisition time. However, when a new algorithm is proposed, the performances are normally assessed with ad-hoc synthetic data and evaluation criteria, and *comparing different approaches can be difficult*. In a clinical perspective this aspect is crucial, as the availability of a comprehensive comparison of available reconstruction methods, highlighting strengths and weaknesses of each approach, might help clinicians in the choice of the most adequate diffusion MRI technique for a specific clinical application. The *high angular resolution diffusion MRI reconstruction challenge* is organized with the aim to provide all researchers in this field with a common framework to assess the performances of their own local reconstruction schemes and fairly compare their results against other approaches under controlled conditions.

The main goal of this contest is to investigate not only the local accuracy in the estimation of the intra-voxel fiber configuration of each algorithm, but also **the effect of the local reconstruction accuracy on subsequent global connectivity analyses**.

ORGANIZING COMMITTEE

The challenge has been organized as a collaboration of the following international institutions:

- ALESSANDRO DADUCCI
  - *Signal Processing Laboratory (LTS5), EPFL, Switzerland*
  - http://people.epfl.ch/Alessandro.Daducci
- EMMANUEL CARUYER
  - *Department of Radiology, University of Pennsylvania, USA*
  - http://www.rad.upenn.edu/sbia/Emmanuel.Caruyer/
- MAXIME DESCOTEAUX
  - *Sherbrooke Connectivity Imaging Lab (SCIL), Université de Sherbrooke, Canada*
  - http://scil.dinf.usherbrooke.ca
- JEAN-PHILIPPE THIRAN
  - *Signal Processing Laboratory (LTS5), EPFL, Switzerland*
    University Hospital Center (CHUV) and University of Lausanne (UNIL), Switzerland
  - http://lts5www.epfl.ch

CONTEST ORGANIZATION

Last year we organized a similar challenge on local reconstruction methods in diffusion MRI. Taking to heart this past experience, some **MAJOR IMPROVEMENTS** have been introduced in this year's edition.

A. More realistic simulation of the diffusion signal

The diffusion MRI signal corresponding to a given intra-voxel configuration has been made more realistic by employing **ADVANCED MODELS** accounting for both intra- and extra- cellular water. The phantom consists in a set of fiber bundles, that connect one area of the "cortex" to another. There is a wide range of configurations (branching, crossing, kissing), fiber bundles radii, and fiber geometry.

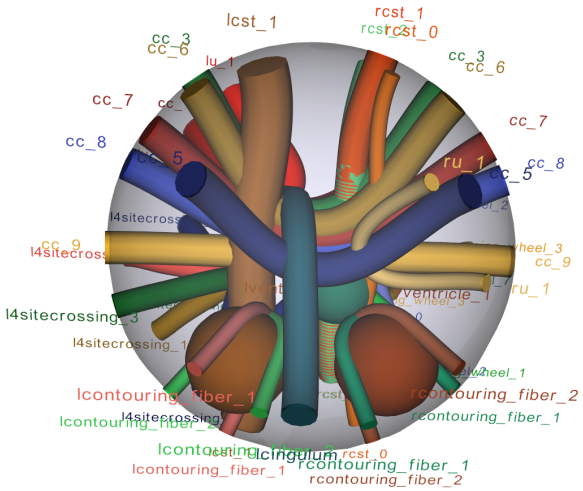

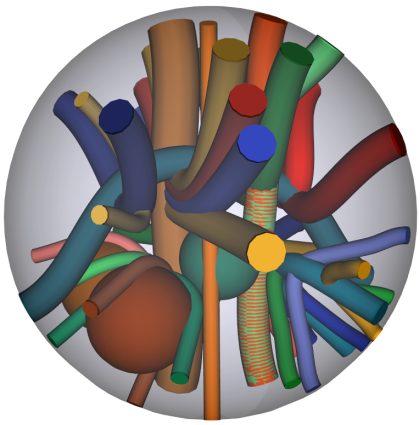

Given the previous fiber configurations, the diffusion MR signal has been simulated in each voxel considering both **hindered and restricted diffusion**, to account for extra-axonal and intra-axonal water. Depending on the position in space, an additional isotropic compartment has been included to model the **CSF contamination** close to the ventricles in brain imaging. To account for the **partial volume effect** (multiple fiber compartments within the same imaging voxel), we used an approach similar to the Numerical Fiber Generator (Close et al, 2009).

Finally, the magnitude diffusion MR signal E has been corrupted by Rician noise as:

$$E_{\text{noisy}} = \sqrt{(E + \eta_1)^2 + \eta_1^2}$$

where η_1 and η_2, are independent, zero-mean Gaussian distributed with the same covariance σ^2.

B. Separate sampling classes

The submissions have been subdivided into THREE DIFFERENT CLASSES, depending on the characteristics of the sampling scheme adopted by each algorithm:

- `DTI-like` : 6-32 samples and $b \leq 1200$ s/mm^2
- `HARDI-like` : 33-64 samples and $1500 \leq b \leq 4000$ s/mm^2
- `Heavyweight` : 65-515 samples and $b \leq 12000$ s/mm^2

A separate ranking has been drawn for each sampling class, therefore identifying three winners.

C. New evaluation system

Two main criteria have been considered to assess the performances of the proposed approaches: the **local accuracy** in the estimation of the fiber configurations and the **global impact** of this accuracy on a subsequent connectivity analysis performed with standard fiber-tracking algorithms.

- AT THE VOXEL LEVEL, a score was attributed accounting for the following metrics:
  - *Correct estimation of the number of fiber compartments*, expressed by means of the probability of false fibre detection:
    $$P_d = \frac{|M_{true} - M_{estimated}|}{M_{true}}$$
    where M_{true} and $M_{estimated}$ are, respectively, the real and estimated number of fiber compartments inside the voxel.
  - *Angular precision of the estimated fiber compartments*, assessed by means of the angular error between the estimated fiber directions and the true ones inside the voxel:
    $$\epsilon_\theta = \arccos(|\vec{d}_{true} \cdot \vec{d}_{estimated}|) \frac{180}{\pi}$$
    where $\vec{d}_{true}$ is a true direction and $\vec{d}_{estimated}$ is its closest estimate. The final value is the average of the angular errors computed for all the true fiber compartments..
- AT THE MACROSCOPIC LEVEL, we were interested also to study the impact on the quality of subsequent global connectivity analyses performed on top of each local reconstruction method. Standard methods commonly used in the literature to perform fiber-tracking have been chosen and the evaluation was performed following the approach of (Côté et al, 2012).

For determining the **final ranking**, however, only the global measures have been used.

CONTEST PARTICIPANTS

DTI-like class

CRL	**Benoit Scherrer, Maxime Taquet, Simon K. Warfield** *Computational Radiology Lab, Department of Radiology, Children's Hospital Boston (USA)*	32 samples $b = 1000$
PSO	**Michael Paquette, Eleftherios Garyfallidis, Samuel St-Jean, Pierrick Coupé, Maxime Descoteaux** *Sherbrooke Connectivity Imaging Lab, Computer Science Department, Université de Sherbrooke (Canada)* *CNRS Laboratoire Bordelais de Recherche en Informatique (LaBRI), Bordeaux (France)*	32 samples $b = 1200$
Dico Learning	**Sylvain Merlet, Emmanuel Caruyer, Rachid Deriche** *Athena Project-Team, INRIA Sophia Antipolis - Méditerraneé (France)* *Section of Biomedical Image Analysis, Department of Radiology, University of Pennsylvania (USA)*	32 samples $b = 1200$
CSD/SDT	**Eleftherios Garyfallidis, Samuel St-Jean, Michael Paquette, Pierrick Coupé, Maxime Descoteaux** *Sherbrooke Connectivity Imaging Lab, Computer Science Department, Université de Sherbrooke (Canada)* *CNRS Laboratoire Bordelais de Recherche en Informatique (LaBRI), Bordeaux (France)*	32 samples $b = 1200$
RW-L1	**Anna Auría, Alessandro Daducci, Jean-Philippe Thiran, Yves Wiaux** *Signal Processing Lab (LTS5), École Polytechnique Fédérale de Lausanne (EPFL) (Switzerland)* *University Hospital Center (CHUV) and University of Lausanne (Switzerland)* *Department of Radiology and Medical Informatics, University of Geneva (Switzerland)*	32 samples $b = 1200$
NLNNSD	**Jian Cheng, Rachid Deriche, Tianzi Jiang, Dinggang Shen, Pew-Thian Yap** *Univerisity of North Carolina at Chapel Hill (USA)* *Athena Project-Team, INRIA Sophia Antipolis - Méditerraneé (France)* *Institute of Automation, Chinese Academy of Sciences (China)*	32 samples $b = 1200$
Alchemists	**Farshid Sepehrband, Jeiran Choupan, Yaniv Gal, David C. Reuten, Zhengyi Yang** *Centre for Advanced Imaging, The University of Queensland (Australia)* *School of Information Technology and Electrical Engineering, The University of Queensland (Australia)*	26 samples $b = 1200$
The HARDI Boys	**R.H.J. Fick, R. Duits, E.J. Creusen, T.C.J. Dela Haije, P.P.W. Ossenblok, B.M. ter Haar Romenij, A. Vilanova** *Eindhoven University of Technology (The Netherlands)* *Kempenhaeghe Center for Epilepsy (The Netherlands)*	32 samples $b = 1200$

HARDI-like class

CS-SHORE	**Sylvain Merlet, Rachid Deriche** *Athena Project-Team, INRIA Sophia Antipolis - Méditerraneé (France)*	63 samples $b \in \{1500, 2500\}$
Dico Learning	**Sylvain Merlet, Emmanuel Caruyer, Rachid Deriche** *Athena Project-Team, INRIA Sophia Antipolis - Méditerraneé (France)* *Section of Biomedical Image Analysis, Department of Radiology, University of Pennsylvania (USA)*	63 samples $b \in \{1500, 2500\}$
Diffusion Water-Frogs	**Ramon Aranda, Mariano Rivera, Alonso Ramirez-Manzanares** *Computer Science Department, Centro de Investigación Matemáticas (CIMAT), A.C (Mexico)* *Universidad de Guanajuato, Department of Mathematics (Mexico)*	64 samples $b = 3000$
Frogs	**Alonso Ramirez-Manzanares, Ramon Aranda, Mariano Rivera, Omar Ocegueda** *Department of Mathematics, Universidad de Guanajuato (Mexico)* *Computer Science Department, Centro de Investigación Matemáticas (CIMAT), A.C (Mexico)*	64 samples $b = 3000$
Blue-Dart Frogs	**Omar Ocegueda, Mariano Rivera** *Computer Science Department, Centro de Investigación Matemáticas (CIMAT), A.C (Mexico)*	64 samples $b = 3000$
PSO	**Michael Paquette, Eleftherios Garyfallidis, Samuel St-Jean, Pierrick Coupé, Maxime Descoteaux** *Sherbrooke Connectivity Imaging Lab, Computer Science Department, Université de Sherbrooke (Canada)* *CNRS Laboratoire Bordelais de Recherche en Informatique (LaBRI), Bordeaux (France)*	64 samples $b = 3000$

CSD/SDT	**Eleftherios Garyfallidis, Samuel St-Jean, Michael Paquette, Pierrick Coupé, Maxime Descoteaux** *Sherbrooke Connectivity Imaging Lab, Computer Science Department, Université de Sherbrooke (Canada)* *CNRS Laboratoire Bordelais de Recherche en Informatique (LaBRI), Bordeaux (France)*	64 samples $b = 3000$
Capablanca	**Erick Jorge Canales-Rodríguez** *FIDMAG Research Foundation, Germanes Hospitaláries, (Barcelona, Spain)* *Centro de Investigación Biomédica en Red de Salud Mental (CIBERSAM), (Madrid, Spain)*	64 samples $b = 3000$
ODF Ten Decomp	**Yaniv Gur, Chris R. Johnson** *SCI Institute, University of Utah (USA)*	60 samples $b = 3000$
STD	**Yaniv Gur, Chris R. Johnson** *SCI Institute, University of Utah (USA)*	60 samples $b = 3000$
NLNNSD	**Jian Cheng, Rachid Deriche, Tianzi Jiang, Dinggang Shen, Pew-Thian Yap** *Univerisity of North Carolina at Chapel Hill (USA)* *Athena Project-Team, INRIA Sophia Antipolis - Méditerraneé (France)* *Institute of Automation, Chinese Academy of Sciences (China)*	64 samples $b = 3000$
The HARDI Boys	**R.H.J. Fick, R. Duits, E.J. Creusen, T.C.J. Dela Haije, P.P.W. Ossenblok, B.M. ter Haar Romenij, A. Vilanova** *Eindhoven University of Technology (The Netherlands)* *Kempenhaeghe Center for Epilepsy (The Netherlands)*	64 samples $b = 3000$

Heavyweight class

CS-DSI	**Sylvain Merlet, Michael Paquette, Rachid Deriche, Maxime Descoteaux** *Athena Project-Team, INRIA Sophia Antipolis - Méditerraneé (France)* *Sherbrooke Connectivity Imaging Lab, Computer Science Department, Université de Sherbrooke (Canada)*	63 samples $b \leq 9600$
DSID/GQID	**Eleftherios Garyfallidis, Michael Paquette, Samuel St-Jean, Pierrick Coupé, Maxime Descoteaux** *Sherbrooke Connectivity Imaging Lab, Computer Science Department, Université de Sherbrooke (Canada)* *CNRS Laboratoire Bordelais de Recherche en Informatique (LaBRI), Bordeaux (France)*	514 samples $b \leq 11540$
NLNNSD	**Jian Cheng, Rachid Deriche, Tianzi Jiang, Dinggang Shen, Pew-Thian Yap** *Univerisity of North Carolina at Chapel Hill (USA)* *Athena Project-Team, INRIA Sophia Antipolis - Méditerraneé (France)* *Institute of Automation, Chinese Academy of Sciences (China)*	514 samples $b \leq 4000$
Spiral	**Farshid Sepehrband, Jeiran Choupan, Yaniv Gal, David C. Reuten, Zhengyi Yang** *Centre for Advanced Imaging, The University of Queensland (Australia)* *School of Information Technology and Electrical Engineering, The University of Queensland (Australia)*	226 samples $b = 2000$

AGENDA

13.30 - 13.40 WELCOME AND OPENING
Alessandro Daducci

13.40 - 13.50 TESTING DATA GROUND-TRUTH AND SIGNAL GENERATION
Emmanuel Caruyer

13.50 - 14.40 KEYNOTE **"Diffusion MRI Processing: Past, Present & Future"**
Baba C. Vemuri

14.40 - 14.50 TALK **"Team report: `Alchemists` and `Spiral`"**
Farshid Sepehrband

14.50 - 15.00 TALK **"Team report: `CSD/SDT`, `DSID/GQID` and `PSO`"**
Eleftherios Garyfallidis and *Michael Paquette*

15.00 - 15.30 COFFEE BREAK

15.30 - 15.40 TALK **"Team report: `CRL`"**
Benoit Scherrer

15.40 - 15.50 TALK **"Team report: `Frogs`, `Blue-dart frogs` and `Diffusion Water-Frogs`"**
Alonso Ramirez Manzanares

15.50 - 16.00 TALK **"Team report: `RW-L1`"**
Anna Auría

16.00 - 16.10 TALK **"Team report: `Dico Learning`, `CS-DSI` and `CS-SHORE`"**
Sylvain Merlet

16.10 - 16.20 TALK **"Team report: `ODF Ten Decomp` and `STD`"**
Yaniv Gur

16.20 - 16.30 TALK **"Team report: `The HARDI Boys`"**
Rutger Fick

16.30 - 16.50 EVALUATION SYSTEM AND RESULTS
Maxime Descoteaux

16.50 - 17.00 WINNERS ANNOUNCEMENT AND CLOSING
Emmanuel Caruyer, Alessandro Daducci, Maxime Descoteaux

PROCEEDINGS

Diffusion MRI Processing: Past, Present & Future*

Baba .C. Vemuri
Professor, Department of Computer & Information Science & Engineering
University of Florida, Gainesville, Florida

Abstract

Diffusion MRI (dMRI) is a relatively nascent non-invasive imaging technique that allows the measurement of water molecular diffusion through tissue *in vivo*. The directional features of water diffusion allow one to infer the connectivity patterns prevalent in tissue and possibly track changes in this connectivity over time for various clinical applications. There are two fundamental quantities that one is normally interested in computing for analysis of dMRI data sets, they are: (i) water molecule displacement probability function and (ii) the diffusivity function. The former is needed in estimating the fiber orientations required in tractography and the latter is used in computing clinically significant quantities such as mean diffusivity, generalized anisotropy etc. In this talk, I will present a brief survey of the state-of-the-art methods for reconstruction of the aforementioned functions indicating where the field is at and what the lies ahead.

*This research was in part funded by the NIH grant NS066340.

Cube and Sphere (CUSP) Diffusion Weighted Imaging

Benoit Scherrer*, Maxime Taquet* and Simon K. Warfield*
* Computational Radiology Laboratory, Department of Radiology
Children's Hospital Boston, 300 Longwood Avenue, Boston, MA, 02115, USA

I. Introduction

Multiple approaches have been proposed to overcome the limitations of diffusion tensor imaging (DTI) and to represent multiple white matter (WM) fascicles in a voxel. Among them, generative models such as multi-tensor models seek to represent the contribution from each WM fascicle and are of great interest to characterize and compare WM properties. They also enable characterization of the freely diffusing water, which enables compensation for CSF contamination and characterization of pathologies such as edema, stroke or inflammation. The estimation of the model parameters is ill-posed with a single non-zero b-value [3]. However, the optimal strategy to image at multiple non-zero b-values remains unclear. For this challenge, we propose to investigate the efficacy of the recently proposed Cube and Sphere (CUSP) gradient encoding scheme. In contrast to a multi-shell acquisition, CUSP achieves a low echo time (TE) and maintains high SNR for each DW image. We focus on a short multiple b-values acquisitions (32 DW-images) achievable with the exact same TE and same acquisition time compared to typical single b-value acquisitions employed in DTI.

II. Material and Method

1) CUSP Imaging: Modification of the b-value in a DW experiment can be achieved by modifying the gradient pulse duration δ, the time separation between the pulses Δ or the gradient strength $||\mathbf{g}||$ as described by $b = \gamma^2\delta^2(\Delta - \delta/3)G^2||\mathbf{g}||^2 = b_{\text{nominal}}||\mathbf{g}||^2$. In the multi-shell HARDI, all shells in q-space are described with the same δ and Δ and varying $||\mathbf{g}||$. Because the components of $\mathbf{g}$ must verify $|g^X| \leq 1, |g^Y| \leq 1, |g^Z| \leq 1$, the largest shell must be described with gradients with $||\mathbf{g}|| = 1$, and other shells with $||\mathbf{g}|| \leq 1$. Achieving a large b-value with $||\mathbf{g}|| = 1$ requires long duration δ and Δ, leading to a long TE and a significant signal dropout due to T2 relaxation for *all* the shells.

In contrast, Cube and Sphere (CUSP) DWI [3] is based on utilizing $||\mathbf{g}|| > 1$ to provide multiple b-values while achieving short TE. Because each component of $\mathbf{g}$ must have norm smaller than one, the set of gradients that can be imaged with fixed δ and Δ and varying $\mathbf{g}$ describes a 3-D cube in q-space, corresponding to a *cube of constant TE*. We first fix δ and Δ to image an inner shell with $||\mathbf{g}|| = 1$ (blue in Fig.1a) that uniformly samples q-space with b-value chosen to provide optimal SNR for imaging the WM ($b_{\text{nominal}} = 1000\text{s/mm}^2$ in an adult brain). We acquire other DW images with gradients on the faces of the cube of constant TE (red in Fig.1a). This provides multiple b-values up to $3b_{\text{nominal}}$ without any cost in SNR due to T2 relaxation.

2) Diffusion model: We consider a multi-fascicle model in which each fascicle is represented by a tensor and the diffusion of free water is represented by an isotropic tensor. This amounts to considering the following generative model for the formation of the diffusion signal S for a b-value b and a gradient direction $\boldsymbol{g}$:

$$S = S_0 \left(f_0 e^{-bD_{\text{iso}}} + \sum_{i=1}^{m} f_i e^{-b\boldsymbol{g}^T \boldsymbol{D}_i \boldsymbol{g}} \right),$$

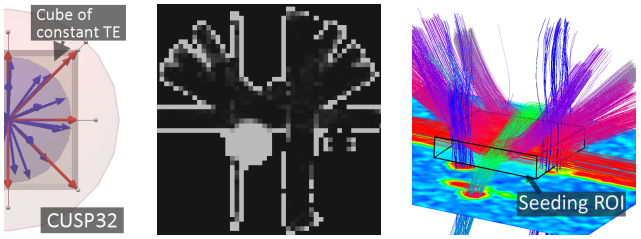

(a) (b) (c)

Fig. 1. CUSP32 employed for this challenge (a). Fraction of isotropic diffusion estimated with the ISBI 30dB phantom, capturing partial volume averaging and unrestricted diffusion (b). Tractography achieved from one seeding ROI with the 30dB phantom, showing multiple crossing regions (c).

where S_0 is the signal with no diffusion gradient applied, D_{iso} the diffusion of free water, f_i the volumetric fractions of occupancy ($\sum_{i=0}^{m} f_i = 1$), m the number of fascicles and $\boldsymbol{D}_i$ the tensor representing the fascicle i.

3) Method: We employed a CUSP32 acquisition with 22 gradients uniformly distributed on the hemisphere at $b = 1000$ and 10 gradients on the cube with $||\mathbf{g}|| > 1$: the four tetrahedral gradients $(\pm 1, \pm 1, \pm 1)$ and the six hexahedral gradients. Each DW image was corrected for noise using an optimized blockwise nonlocal means denoising filter [1]. The model parameters were estimated using a maximum *a posteriori* approach [3]. We focused on models complexity ranging from $m = 0$ (isotropic diffusion) to $m = 3$ fascicles. Critical to the accurate estimation of the model parameters is the model order selection. Here, we employed a recently proposed approach based on the minimization of the generalization error assessed with the Bootstrap 632 method [2].

III. Discussion

The very low number of DW images considered makes it challenging to achieve both model order selection and estimation of the model parameters. Recent developments have addressed these challenges by careful consideration of the image acquisition process [3], image pre-processing [1] and DW signal modeling [2], [3]. This enables accurate estimation of the model parameters from a small number of DW images. This will provide the opportunity of investigating the WM architecture from a short duration DWI acquisition, both in research and clinical practice.

References

[1] Coupe, P., Yger, P., Prima, S., Hellier, P., Kervrann, C., Barillot, C.: An optimized blockwise nonlocal means denoising filter for 3-d magnetic resonance images. IEEE Trans Med Imaging 27(4), 425–441 (2008)
[2] Scherrer, B., Taquet, M., Warfield, S.K.: Reliable Selection of the Number of Fascicles in Diffusion Images by Estimation of the Generalization Error. IPMI (2013)
[3] Scherrer, B., Warfield, S.K.: Parametric Representation of Multiple White Matter Fascicles from Cube and Sphere Diffusion MRI. PLoS ONE 7(11) (2012)

Compressive Sensing DSI

Sylvain Merlet*, Michael Paquette†, Rachid Deriche* and Maxime Descoteaux†
* Athena Project-Team, INRIA Sophia Antipolis - Méditerranée, France
† Sherbrooke Connectivity Imaging Laboratory, Computer Science Department, Université de Sherbrooke

***Abstract*—Compressive Sensing (CS) [2], [1] offers an efficient way to decrease the number of measurements required in Diffusion Spectrum Imaging (DSI). This method aims to reconstruct the Ensemble Average Propagator (EAP) and, for the purpose of this contest, we compute the numerical Orientation Distribution Function (ODF) by integrating the EAP over a solid angle. In this abstract, we briefly describe three important points underlying the CS technique in order to accelerate DSI, namely the sparsity, the Restricted Isometry Property (RIP) and the ℓ_1 reconstruction scheme. Due to the high b-values required in the sampling protocol, our approach enters the heavyweight sampling category. Nevertheless, only 64 measurements are used for the reconstruction.**

I. Sparse representation of the EAP

A sparse representation of the EAP is one of the key ingredient of an efficient CS recovery. In this work, we use the Discrete Wavelet Transform (DWT) based on the biorthogonal Cohen-Daubechies-Feauveau (CDF) 9-7 wavelet in order to sparsely describe the EAP. It has been shown that the CDF 9-7 wavelet leads to a very sparse representation of the EAP [4], [5]. In Fig. 1, we show the decomposition scaling and wavelet functions.

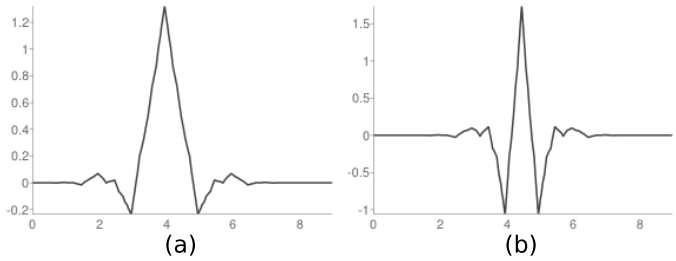

Fig. 1. The CDF 9-7 wavelet. (a) Decomposition scaling function. (b) Decomposition wavelet function.

II. The Restricted Isometry Property (RIP)

The RIP property is respected with a high probability when the acquisition are taken at random [1]. The possibility to acquire q-space samples in a random fashion is an important aspect in DSI that facilitates the application of the CS technique. In Fig. 2, we show an example of random sampling scheme.

In practice, since the diffusion signal is antipodally symmetric, we generate the sampling scheme in half the grid and then symmetrize it. For the contest we asked for 64 measurements in order to compare our results with HARDI-like reconstruction. However, because we require high b-values in the acquisition protocol we enter the heavyweight sampling category.

III. The ℓ_1 reconstruction scheme

The solution x of our problem is given by solving the following convex optimization problem [3], [1] :

$$argmin_x J(x) = \|TF_{u0}(x) - E_u\|_2^2 + \lambda\|\Psi x\|_1 \qquad (1)$$

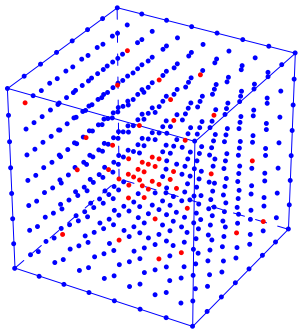

Fig. 2. 3D random sampling scheme. The blue points represent a full sampling of the 3D cartesian grid. The red points are samples taken at random.

The first term is the data consistency constraint, $\|\Psi x\|_1$ is the sparsity constraint with Ψ an operator representing the CDF 9-7 wavelet based DWT. λ is the Lagrange parameter that defines the confidence we put in the measured signal E_u. The data consistency constraint enables the solution to remain close to the raw data acquisition. TF_{u0} is the 3D undersampled Fourier operator defined by three operations. The first operation consists in applying a 3D Fourier transform. The latter is undersampled in a random manner. Then, the other coefficients are replaced by zero values. Hence, the acquired data are defined by $E_u = TF_{u0}(P)$ with P the propagator to be recovered. x is the estimated propagator so $TF_{u0}(x)$ is the undersampled Fourier transform of the estimated propagator. Equation (1) finds the sparsest solution with respect to Ψ that corresponds to the acquired data.

IV. Technical aspect regarding the ODF computation

In order to obtain the ODFs, we do not integrate between 0 and and R_{max} (the maximum radius of the EAP in the 3D cartesian grid). Instead, we integrate the EAPs between the range $[R_{\text{max}} \times \alpha, R_{\text{max}} \times \beta]$ with $\alpha, \beta \in [0, 1]$, because we observed that well chosen bounds for the radial integration lead to better results in terms of DNC and AE. Based on previous experiments, we choose $\alpha = 0.2$ and $\beta = 0.7$.

References

[1] E.J. Cands and M.B. Wakin. An introduction to compressive sampling. *Signal Processing Magazine, IEEE*, 25(2):2130, 2008.
[2] D.L. Donoho. Compressed sensing. *Information Theory, IEEE Transactions on*, 52(4):1289–1306, 2006.
[3] M. Lustig, D. Donoho, and J.M. Pauly. Sparse mri: The application of compressed sensing for rapid mr imaging. *Magnetic Resonance in Medicine*, 58(6):11821195, 2007.
[4] Sylvain Merlet, Michael Paquette, Rachid Deriche, and Maxime Descoteaux. Ensemble average propagator reconstruction via compressed sensing: Discrete or continuous bases ? In *ISMRM 20th Annual Meeting (2012)*, page 2277, Australie, May 2012.
[5] Etienne Saint-Amant and Maxime Descoteaux. Sparsity characterization of the diffusion propagator. In *Proceedings of ISMRM*, 2011.

Continous signal recovery via the SHORE basis

Sylvain Merlet*, Rachid Deriche*
* Athena Project-Team, INRIA Sophia Antipolis - Méditerranée, France

***Abstract*—We exploit the ability of Compressed Sensing (CS) to recover the whole 3D Diffusion MRI (dMRI) signal from a limited number of samples while efficiently recovering the Orientation Distribution Function (ODF). We first present the orthonormal basis used to model the diffusion signal, namely the SHORE basis, along with an analytical formula to estimate the ODF. Next, we describe the sampling protocol sent to the contest organizers. The last section describes the ℓ_1-minimization use in CS reconstruction. The method is fully described in [4].**

I. Diffusion signal modeling in the SHORE basis

We represent $E(q\mathbf{u})$ as a truncated linear combination of SHORE basis function $\Phi_{n\ell m}(q\mathbf{u})$ with n the radial order, ℓ and m the angular order and degree,

$$E(q\mathbf{u}) = \sum_{n=0}^{N}\sum_{\ell=0}^{L}\sum_{m=-\ell}^{\ell} c_{n\ell m}\Phi_{n\ell m}(q\mathbf{u}), \tag{1}$$

where the $c_{n\ell m} = \langle E, \Phi_{n\ell m}\rangle$ are the transform coefficients. Several others bases can be used to continuously reconstruct the diffusion signal. [4] points out the efficiency of the SHORE basis in resolving the CS problem. That is why we decided to use this basis to perform our reconstruction.

The SHORE basis has been introduced by [5] but the basis was only orthogonal. [2] proposed a new formulation where the basis functions have a l_2 norm equal to one. This orthonormal basis is expressed as,

$$\Phi^{(\text{SHORE})}_{n\ell m}(q\mathbf{u}) = \left[\frac{2(n-\ell)!}{\zeta^{3/2}\Gamma(n+3/2)}\right]^{1/2}\left(\frac{q^2}{\zeta}\right)^{l/2}\exp\left(\frac{-q^2}{2\zeta}\right)L^{l+1/2}_{n-\ell}\left(\frac{q^2}{\zeta}\right)Y^m_\ell(\mathbf{u}). \tag{2}$$

Note that, because the Laguerre polynomial order ($n-\ell$ in Eq. 2) must be positive, the angular order ℓ depends on the radial order n, such that $n \geq \ell$. Then, the angular order ℓ is bounded by n.

Defining the ODF Υ as the integration of the EAP over a solid angle, a closed formula for the ODF has been derived in terms of real and symmetric Spherical Harmonic (SH) basis functions :

$$\Upsilon(\mathbf{r}) = \sum_{\ell=0}^{L}\sum_{m=-\ell}^{\ell} \upsilon_{\ell m}Y^m_\ell(\mathbf{r}), \tag{3}$$

where $Y^m_\ell(\mathbf{u})$ is the SH function of order ℓ and degree m. The coefficients $\upsilon^{(\text{SHORE})}_{\ell m}$ are express as

$$\upsilon^{(\text{SHORE})}_{\ell m} = \sum_{n=0}^{N} c_{n\ell m}\frac{(-1)^{n-l/2}}{2(4\pi^2\zeta)^{3/2}}\left[\frac{2(4\pi^2\zeta)^{3/2}(n-l)!}{\Gamma(n+3/2)}\right]^{1/2} \frac{\Gamma(\ell/2+3/2)\Gamma(3/2+n)}{\Gamma(l+3/2)(n-l)!}\left(\frac{1}{2}\right)^{-\ell/2-3/2} {}_2F_1(-n+l, l/2+3/2; l+3/2; 2), \tag{4}$$

where ${}_2F_1$ is the Gauss hypergeometric function.

II. Acquisition protocols

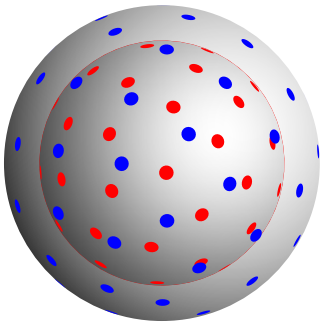

We use a multiple shells sampling scheme with 64 measurements spread on 2 shells at b-values $b = 1500, 2500$ s $\cdot$ mm^{-2} (see figure on the right). We use the algorithm given in [1] by setting the parameters in such a way that the number of points on each shell is proportional to q^1. These particular parameters have been proved efficient in [1], [3]. An important advantage of this algorithm is that the points from each shell have staggered directions and follow a near-optimal uniform distribution. You can generate and download sampling schemes for multiple Q-shell diffusion MRI with this web application : *http://www-sop.inria.fr/members/Emmanuel.Caruyer/q-space-sampling.php*.

III. Sparse reconstruction

Now, we are able to recover any sparse representation $\mathbf{c}$ of a diffusion signal $\mathbf{s}$ with respect to the SHORE basis $\mathbf{\Phi}$ by solving the LASSO problem :

$$\min_{\mathbf{c}} \|\mathbf{s} - \mathbf{\Phi c}\|_2^2 + \lambda\|\mathbf{c}\|_1. \tag{5}$$

We solve 5 via the coordinate descent algorithm.

References

[1] Emmanuel Caruyer, Jian Cheng, Christophe Lenglet, Guillermo Sapiro, Tianzi Jiang, and Rachid Deriche. Optimal design of multiple q-shells experiments for diffusion mri. In *MICCAI Workshop on Computational Diffusion MRI - CDMRI'11*, Toronto, Canada, September 2011.

[2] Jian Cheng, Tianzi Jiang, and Rachid Deriche. Theoretical analysis and practical insights on eap estimation via a unified hardi framework. In *MICCAI workshop on Computational Diffusion MRI*, 2011.

[3] Sylvain Merlet, Emmanuel Caruyer, and Rachid Deriche. Impact of radial and angular sampling on multiple shells acquisition in diffusion mri. In *MICCAI*, volume 6891, pages 113–121. Springer, 2011.

[4] Sylvain Merlet and Rachid Deriche. Continuous diffusion signal, eap and odf estimation via compressive sensing in diffusion mri. *Medical Image Analysis*, 2012. To be published.

[5] E. Ozarslan, C.G. Koay, T.M. Shepherd, S.J. Blackband, and P.J. Basser. Simple harmonic oscillator based reconstruction and estimation for three-dimensional q-space mri. In *ISMRM 17th Annual Meeting and Exhibition, Honolulu,*, page 1396, 2009.

Parametric Dictionary Learning

Sylvain Merlet*, Emmanuel Caruyer† and Rachid Deriche*
* Athena Project-Team, INRIA Sophia Antipolis - Méditerranée, France
† Section of Biomedical Image Analysis, Department of Radiology, University of Pennsylvania

***Abstract*—We recently developed a parametric dictionary learning algorithm and exploited the sparse property of the designed dictionary to recover the diffusion signal and some important diffusion features with a reduced number of measurements. In particular, we derived a closed-form expression to estimate the Orientation Distribution Function (ODF). We present our approach as follows. The first section briefly describes the computational framework used to model the diffusion signal along with the ODF. The full description of the parametric dictionary algorithm is given in [4]. Next, we present the two sampling schemes used for reconstructing the testing data. The first one considers just one shell with 32 measurements and the second one considers multiple shells with 64 measurements. We, thus, enter both the DTI and the HARDI sampling classes. The dictionary together with these two sampling are used to efficiently solve an ℓ_1-minimization problem underlying the sparse reconstruction. The last section presents the mathematical aspect of this problem.**

I. Continuous diffusion modeling with a constrained dictionary

We represent the diffusion signal $E(\mathbf{q})$ as a linear combination of dictionary atoms $\Psi_k(\mathbf{q})$,

$$E(\mathbf{q}) = \sum_{k=0}^{K} c_k \Psi_k(\mathbf{q}), \tag{1}$$

where the $c_{n\ell m} = \langle E, \Phi_{n\ell m} \rangle$ are the transform coefficients.

The complete description of each atom Ψ_k of the dictionary is given by :

$$\begin{aligned}\Psi_k(\mathbf{q}) = \Psi_k(q\mathbf{u}) &= \frac{1}{\sqrt{\chi_k}} \sum_{i=0}^{I} \alpha_{ki} \exp\left(-\nu_{ki} q^2\right) \sum_{j=0}^{J} \beta_{kij} q^{l(j)} Y_j(\mathbf{u}) \\ &= \frac{1}{\sqrt{\chi_k}} \sum_{i=0}^{I} \sum_{j=0}^{J} \gamma_{kij} \exp\left(-\nu_{ki} q^2\right) q^{l(j)} Y_j(\mathbf{u}) \\ &= \Psi_k(\boldsymbol{\gamma_k}, \boldsymbol{\nu_k}, q\mathbf{u}), \end{aligned} \tag{2}$$

with $\mathbf{q}$ the 3D effective gradient, $\mathbf{u}$ an unitary vector and q the norm of the effective gradient such that $\mathbf{q} = q\mathbf{u}$. I and J are, respectively, the radial order and the angular order of the dictionary. J also corresponds the total number of spherical harmonic (SH) taken into account in the modeling not to be confused with the maximal SH order L. Indeed, J is directly related to the maximal SH order L as $J = (L+1)(L+2)/2$. $Y_j(\mathbf{u})$ is the SH of order $l(j) = 0$ for $j = 1$, $l(j) = 2$ for $j \in \{2, ..., 6\}$, $l(j) = 4$ for $j \in \{7, ..., 15\}$ ... . $\boldsymbol{\gamma_k} = \{\gamma_{kij}\}_{i=0...I, j=0...J}$ and $\boldsymbol{\nu_k} = \{\nu_{ki}\}_{i=0...I}$ are two vectors of parameters, which will be set during the learning process. The term $q^{l(j)}$ ensures the continuity of Ψ_k at zero. χ_k is a constant, which ensures the normalization of Ψ_k for the ℓ_2 norm, i.e $\sqrt{\int_{\mathcal{R}^3} \Psi_k^2(\mathbf{q}) d\mathbf{q}} = 1$,

$$\chi_k = \sum_{i'=0}^{I} \sum_{i=0}^{I} \sum_{j=0}^{J} \frac{\gamma_{kij}\gamma_{ki'j}}{2(\nu_{ki} + \nu_{ki'})^{\ell(j)+3/2}} \Gamma\left(\ell(j) + \frac{3}{2}\right), \tag{3}$$

with Γ the gamma function.

Contest parameters: For the contest, we set $I = 2$ and $J = 28$, i.e. a SH order $L = 6$. The dictionary was learned on the voxels of the training data with a fractional anisotropy $FA > 0.2$. This leads to a dictionary of 120 atoms.

II. Acquisition protocols

To obtain the single shell sampling scheme, we use the static repulsion algorithms [2] to uniformly distribute points on a sphere. We choose a b-value $b = 1200$ s $\cdot$ mm^{-2}.

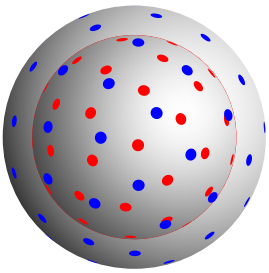

The second scheme is a multiple shells sampling scheme with 64 measurements spread on 2 shells at b-values $b = 1500, 2500$ s $\cdot$ mm^{-2} (see figure on the right). We use the algorithm given in [1] by setting the parameters in such a way that the the number of points on each shell is proportional to q^1. These particular parameters have been proved efficient in [3], [1]. An important advantage of this algorithm is that the points from each shell have staggered directions and follow a near-optimal uniform distribution. You can generate and download sampling schemes for multiple Q-shell diffusion MRI with this web application : *http://www-sop.inria.fr/members/Emmanuel.Caruyer/q-space-sampling.php*.

III. Sparse reconstruction

From the dictionary designed via the algorithm given in [4], we can recover any sparse representation $\mathbf{c}$ of a diffusion signal $\mathbf{s}$ with respect to $\mathbf{D}$ by solving the LASSO problem :

$$\min_{\mathbf{c}} \|\mathbf{s} - \mathbf{D}\mathbf{c}\|_2^2 + \lambda \|\mathbf{c}\|_1. \tag{4}$$

We solve 4 via the coordinate descent algorithm.

References

[1] E. Caruyer, C. Lenglet, G. Sapiro, and R. Deriche. Design of multi-shell sampling schemes with uniform coverage in diffusion mri. *MRM*, 2013. In press.

[2] D.K. Jones, M.A. Horsfield, and A. Simmons. Optimal strategies for measuring diffusion in anisotropic systems by magnetic resonance imaging. *Magnetic Resonance in Medicine*, 42(39):515 – 525, August 1999.

[3] Sylvain Merlet, Emmanuel Caruyer, and Rachid Deriche. Impact of radial and angular sampling on multiple shells acquisition in diffusion mri. In *MICCAI*, volume 6891, pages 113–121. Springer, 2011.

[4] Sylvain Merlet, Emmanuel Caruyer, and Rachid Deriche. Parametric dictionary learning for modeling eap and odf in diffusion mri. In *Lecture Notes in Computer Science series MICCAI 2012*, volume 7512, page 7512, Nice, France, October 2012.

Diffusion Water-Frogs Team Report: Self-Oriented Diffusion Basis Functions

Ramon Aranda†, Mariano Rivera† and Alonso Ramirez-Manzanares*
†Centro de Investigacion en Matematicas, Department of Computer Science.
* Universidad de Guanajuato, Department of Mathematics

I. Introduction

Water diffusion estimation in cerebral tissue is a noninvasive method for inferring the axon fiber pathways and brain connectivity patterns *in-vivo*, which are two of the most challenging goals in neuroimaging. Several methods have been developed to recover the axonal intra-voxel diffusion information in the multifiber case. Some strategies are based on a dictionary of diffusion basis functions (DBF) [1]. The DBF methods assume that the observed DW-MRI signal at each voxel is a linear combination of a fixed set of diffusion tensor functions whose orientations are uniformly distributed along the unit sphere. Since the functions are generated from fixed orientations they do not necessarily correspond to the actual fiber orientations. To overcome this limitation, we recently developed an extension to the DBF method to reorient the elements of the dictionary towards the most plausible fiber directions. In this work, we present the result of our Self-Oriented DBF model on the 2013 HARDI Reconstruction Challenge data set.

II. Self-Oriented DBF Model

We define the new DBF formulation as follow:

$$\phi_{i,k} = S_0 \exp\left(-b g_i^T R(\theta_k) \bar{T}_k R(\theta_k)^T g_i\right), \tag{1}$$

where R is a 3D rotation matrix defined by the angles $\theta_k = [\theta_{x,k}, \theta_{y,k}, \theta_{z,k}]$. When $\theta_k = [0,0,0]$ this formulation corresponds to the proposal in [1]. We are interested in computing the angular displacement θ_k to align the Principal Diffusion Direction (PDD) of $\bar{T}_k$ with the actual fiber orientation according to the DW-MRI signal. To this aim, we propose to compute the angular displacement by:

$$\begin{aligned} \min_{\Theta,\alpha} \quad & U(\Theta,\alpha) = \|\Phi(\Theta)\alpha - S\|_2^2 \\ \text{subject to} \quad & \alpha \geq 0, \end{aligned} \tag{2}$$

where $\Theta = \{\theta_k\}_{k=1,\ldots,N}$ and $\Phi(\Theta) = \{\phi_{i,k}\}_{i=1,\ldots,M, k=1,\ldots,N}$. The direct minimization of (2) can be complicated. Therefore, we propose an alternative minimization approach as follows: to solve iteratively a quadratic program for α (fixing Θ) and then a non-linear program for Θ (fixing α). Notice that for a fixed Θ, the equation (2) is a non-negativity least squares problem, which can be solved easily. Solving for Θ is not so direct because R is constrained to be a rotation matrix. However, we can simplify the problem rewriting R as the product of three rotation matrices in terms of the cosine directors around the canonical axis. Then if we constrain such rotational angles in θ_k to be small it is possible to use the approximations: $\cos(\theta) = 1$ and $\sin(\theta) = x$. Moreover, if only one ration matrix is applied at the same time, we can solve for Θ by means of three simpler optimizations problems (for more details see [2]).

This work is supported in part by 131369, 169338, 169178, 131771 grants from CONACYT, Mexico. R. Aranda was also supported by a Ph.D. scholarship from CONACYT, Mexico.

III. Hardi Reconstruction contest

In order to estimate the intra-voxel information, we adopted an acquisition protocol composed of 64 diffusion-weighted images with an homogeneous b = 3000 value. For the self-oriented model, we use a set of 256 equally distributed orientations into the 3D unitary sphere.

A. White Matter Segmentation

Since the analysis of the *Fractional Anisotropy* map of the phantom data did not clearly indicate the white matter structure, we note that with the average of the DW-MRI signals was possible to have a correct segmentation. Additionally, we detect the presence of potential *water structures*. To distinguish between the water structure and white matter, we perform an analysis of local coherence of each voxel with respect to its neighborhood. We define the local coherence value as the average on the angular errors between the estimated *peaks* in each voxel and its neighborhood. After we compute the local coherence values for the complete data, we spatially smooth them with an homogeneous filtering process. Then, voxels with a local coherence > 15 degrees is marked as water.

B. Proposed Solution

In our experiment, we note that use only the information of the basis diffusivity profile found by the DBF model ($\lambda_1 > \lambda_{2,3}$) and the *peaks* to generated the ODF does not provide competitive results for some tractography methods. For this reason, we provide both the *peaks* and the *spherical harmonics representation* of the estimated ODF as follows:

- Peaks: we allow a maximum of three peaks per voxel. In addition, In order to overcome the overestimation of peaks, we eliminate the basis tensors with a size compartment smaller than 25% of the biggest size compartment within a voxel.
- ODF: to generate the ODF, we do thinner the basis diffusivity profile. To this aim, we use the parallel diffusion equal to $4\lambda_1$ and $0.25\lambda_{2,3}$ for the radial diffusion.

Note that for all voxels labeled as water, we set to zeros the number of estimations compartments because the peaks are random and do not provides white matter information. For the ODF case, we set balls as in our experiments we note this strategy improves the connectivity index.

References

[1] A. Ramirez-Manzanares, M. Rivera, B.C. Vemuri, P. Carney and T. Mareci, "Diffusion Basis Functions Decomposition for Estimating White Matter Intravoxel Fiber Geometry", IEEE Trans. Med. Imag., 26, 1091–1102 (2007).

[2] R. Aranda, M. Rivera, and A. Ramirez-Manzanares, "Self-Oriented Diffusion Basis Functions for White Matter Structure Estimation", Proc. in ISBI (2013).

Frogs Team Report: DBFs with Contrasted ODF

Alonso Ramirez-Manzanares*, Ramon Aranda†, Mariano Rivera† and Omar Ocegueda†
* Department of Mathematics, Universidad de Guanajuato
† Computer Science Department, Centro de Investigación en Matemáticas (CIMAT), A.C

I. Introduction

In the last years several methods have been developed in order to recover the axonal intra-voxel diffusion information on brain white matter (WM) from Diffusion Weighted (DW) MRI. Some methods based their reconstruction on a diffusion dictionary and the best as possible atom selection method to explain the DW-MRI signal into a voxel [1], [3]. In particular our group have developed methods based on previous strategy, which also introduce intra and inter voxel regularization of the diffusion profiles [1]. The method in [1] showed an excellent perfomance in last year Challenge; since the method comparisson rules have changed then we considered appropriate to present the DBF method's reconstruction results as baseline in the HARDI 2013 Challenge. We introduce a slight variant in the original formulation to control the tractografy in partial volume voxels.

II. Methods

A. DW Spatial Smoothing

We apply a denoising step on the DW-MRI signals as we explain in the following. It is well known that the DW-MRI signal averaging over similar WM voxels attenuates the acquisition noise and improves intra–voxel information estimation. Given a voxel at a 3D position $r = [x, y, x]$ we take into account the set of 26 voxels belonging to its second-order 3D neighborhood $\mathcal{N}_r$. We filter the DW-MR signal vector using an homogeneous spatial averaging:

$$\hat{S}_r = \frac{1}{\#\mathcal{N}_r + 1}\left(S_r + \sum_{t:t\in\mathcal{N}_r} S_t\right). \quad (1)$$

We observed on the training data that this simple filtering provides an improvement similar to other more–sophisticated methods.

B. The DBF Method

We avoid the complex non-linear optimization problem associated to the fitting of the of Gaussians Mixture Model (GMM) to the DW signal. For this reason, our group proposed a strategy for recovering multi-DTs at axonal fiber crossing regions [1]. We simplify the problem by using a fixed set of Diffusion Basis Functions (DBF) $\Phi = [\phi_{1,1}, \phi_{2,1}, ..., \phi_{L,P}]$ (where L is the total number of applied gradients and P is the total number of base tensors). This set is not complete because is a discretization of the 3D space. $\phi_{i,p}$ is the diffusion weighted signal associated to the gradient vector g_i and a fixed tensor base $\bar{T}_p$. By using this model it is possible to estimate the GMM by solving a linear equation system with constrains. A limitation of this approach is that the diffusion profile for each axon bundle is not estimated: only an average diffusion profile is reported for all the voxels. To transform the solution from the discrete space (the DBF dictionary) to the continuos 3D orientation space we use the clustering heuristic reported on [1].

This work was supported in part by grants and scholarships from CONACyT, México.

III. Implementation Details and Parameters

We use an acquisition protocol composed of 64 diffusion encoding orientations with an homogeneous $b = 3000$ value.

The diffusion ROI was obtained as follows. By analysing the Mean Diffusion (MD) map, we detect the presence of three potential water structures on the phantom, which are "kissing" some WM structures. The water structures were segmented on the MD map based on their hyper–intense feature by using the human assisted ITK-SNAP software [4]: we initialize a 3D snake on the center of the water balls and use the default parameters for the snake evolution for the data with 10, 20 and 30 SNR values. The obtained segmenation separates the well defined water voxels and leaves the partial volume voxels with WM-Water as part of the ROI. The WM region was also segmented on the ITK-SNAP software based on their intensity on the MD map, for this segmentation we set the *curvature force* parameter of the 3D snake to *detailed* in order to recover all the structure details.

The DBF dictionary is composed of 129 directions quasi-uniformly distributed over the half–sphere. Based on previous studies [2] , we know that the DBF method is prone to over estimate the number of diffusion compartments. In order to overcome the overestimation behavior we eliminate Multi-DTs with a size compartment smaller than 20% of the biggest size compartment within a voxel. In the discrete–to–continuos–orientation DBF step, we set a 6-size neighborhood on the basis directions.

For the contest we provide both the Principal Diffusion Direction (PDD) data and the Orientation Distribution Function (ODF) for each voxel. The PDD data is straighforward computed from the DBF solution. Our experiments indicated that it is convenient to increase the constrast of the ODF shape in order to obtain better tractography results, thus, we changed the diffusion profile of the DBF solution: the ODF is computed with $4\lambda_1$ for the parallel diffusion and $\frac{1}{2}\lambda_{2-3}$ for the radial diffusion, where λ_1 and λ_{2-3} are the original DBF parallel and radial diffusion values, respectivelly. The background of the image was filled with *Quiet Not-A-Number* (QNAN) values to stop the tractography methods. The water balls are filled a) with zeros for the PDD solution, and b) with the harmonic spheric representation of isotropic balls for the ODF solution.

References

[1] A. Ramirez-Manzanares , M. Rivera, B. C. Vemuri, P. Carney and T. Mareci, "Diffusion basis functions decomposition for estimating white matter intravoxel fiber geometry", IEEE Trans. Med. Imaging., 26(8), 1091–1102 (2007).

[2] A. Ramirez-Manzanares, P. A. Cook, M. Hall, M. Ashtari and J. C. Gee, "Resolving Axon Fiber Crossings at Clinical b-values: An Evaluation Study", Journal of Medical Physics, 38(9), 5239-53 (2011).

[3] B. Jian, B. C. Vemuri, "A unified computational framework for deconvolution to reconstruct multiple fibers from DW-MRI", IEEE Trans. Med. Imaging., 26(11), 1464–1471, (2007).

[4] P. A. Yushkevich, J. Piven, H. C. Hazlett, R. G. Smith, S. H., J. C. Gee, and G. Gerig. "User-guided 3D active contour segmentation of anatomical structures: Significantly improved efficiency and reliability". Neuroimage 31(3), 1116-28, (2006).

Handling Reconstruction Uncertainty in Multi-Tensor Fields

Omar Ocegueda and Mariano Rivera
Centro de Investigacion en Matematicas (CIMAT), A.C.

I. Introduction

One of the most successful approaches developed to overcome the limitations of the Diffusion Tensor model, especially its incapability of resolving fiber crossings, is the Multi-Tensor (MT) Model developed by Tuch *et al.* [2]. The MT model rely on the assumption that the local geometric structure at the voxel of interest can be described using a set of local orientations that correspond to one or more crossing fiber bundles. When this assumption is not satisfied or the model is unable to explain the complexity of the local structure the resulting fitted model lacks meaningful interpretation. In this work, we explore the possibility to exploit the spatially-uncorrelated behavior of the MT model at highly complex, regions of the brain.

II. Methods

A. Local Coherence Index

We define the *best assignment* of compartments between two neighboring voxels v, w as a mapping $B_{v,w}$ between compartments from voxel v to compartments from voxel w such that the sum of the angles between the corresponding orientations is minimized. That is, $B_{v,w}$ minimizes $\sum_{i=1}^{K} A(T_i(v), T_{i'}(w))$ where K is the number of compartments, $i' = B_{v,w}(i)$, $T_i(v)$ is the *principal diffusion direction* (PDD) of the i-th compartment at voxel v, and $A(x, y)$ denotes the angle between vectors x, y. The *Local Coherence Index* (LCI) at voxel v is defined as

$$\frac{1}{|\mathcal{N}(v)|} \sum_{w \in \mathcal{N}(v)} \frac{1}{K} \sum_{i=1}^{K} A(T_i(v), T_{i'}(w)) \tag{1}$$

where $i' = B_{v,w}(i)$ and $\mathcal{N}(v)$ is the set of neighboring voxels of v. Figure 1 (a) depicts an example of a MT model fitted to signals at an unstructured region. Since the orientations of the compartments' pdd's are highly uncorrelated, the average angle between the neighboring pdd's (the "LCI") is higher than the average angle at well structured regions (fig. 1 (b)), this information can be used as a measure of uncertainty of the local reconstruction. We replaced the fitted ODF of voxels with high LCI with uniform distributions to avoid using unreliable information during tracking (fig. 1 (c)).

B. Local Reconstruction

We used a variation of the Diffusion Basis Functions method developed by A. Ramírez *et al.* [1]. Under this model, a dictionary of N diffusion functions is used, so that the reconstruction problem may be casted as a nonnegative least squares problem at each voxel position p:

$$\beta_p^* = \min_{\beta_p \in \Re^N} ||\Phi\beta_p - S_p||_2^2, \ s.t. \ \beta_p \geq 0, \tag{2}$$

This work was supported in part by CONACYT México.

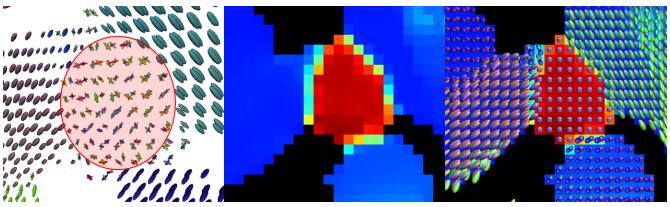

(a) (b) (c)

Fig. 1: (a) Result of fitting a MT model to an unstructured region surrounded by fiber bundles. (b) LCI computed along the region shown in (a), small values are depicted in blue and high values in red. (c) ODF field along the region from (b), the ODF's at highly incoherent voxels was replaced with a uniform distribution.

where $\Phi = [\phi_1, \phi_2, ..., \phi_N]$ is the dictionary of diffusion functions evaluated at a set of N diffusion directions. Each column ϕ_j is characterized by one diffusion tensor D_j whose eigenvalues are assumed to be constant and are estimated using a set of signals from voxels containing one single fiber orientation. The set of dominant peaks at voxel p, can be reliably estimated from the solution β_p^* of eq. (2) using the clustering heuristic proposed in [1], while the ODF can be computed analytically from β_p^*.

C. Regularization

Instead of promoting the parameters β_p^* to be smooth along the volume (*i.e.,* regularizing the parameter field), we enforce each parameter vector β_p^* at voxel p to explain not only the signal observed at voxel p but its neighbors $q \in \mathcal{N}(p)$ as well. Under this perspective, the problem can be formulated as

$$\min_{\beta_p \in \Re^N} \sum_{q \in \mathcal{N}(p) \bigcup \{p\}} ||\Phi\beta_p - S_q||_2^2, \ s.t. \ \beta_p \geq 0, \tag{3}$$

which can be shown to be equivalent to

$$\min_{\beta_p \in \Re^N} ||\Phi\beta_p - \bar{S}_p||_2^2, \ s.t. \ \beta_p \geq 0, \tag{4}$$

where $\bar{S}_p = \frac{1}{1+\mathcal{N}(p)} \sum_{q \in \mathcal{N}(p) \bigcup \{p\}} S_q$, the average of the signals at voxel p and its neighbors.

Our reconstructions were obtained using the HARDI acquisition scheme composed of 64 diffusion encoding gradients with b = 3000.

References

[1] A. Ramirez-Manzanares, M. Rivera, B. C. Vemuri, P. Carney, and T. Mareci. Diffusion basis functions decomposition for estimating white matter intravoxel fiber geometry. *IEEE TMI*, 26(8):1091–1102, 2007.

[2] D. Tuch, T. Reese, M. Wiegell, N. Makris, J. Belliveau, and V. Wedeen. High angular resolution diffusion imaging reveals intravoxel white matter fiber heterogeneity. *MRM*, 48(4):577–82, Oct. 2002.

Particle Swarm Optimization in Multi-Tensor Imaging

Michael Paquette*, Eleftherios Garyfallidis*, Samuel St-Jean*, Pierrick Coupé†, Maxime Descoteaux*
* Sherbrooke Connectivity Imaging Lab (SCIL), Computer Science Department, Université de Sherbrooke, Sherbrooke, Canada
† CNRS Laboratoire Bordelais de Recherche en Informatique (LaBRI), Bordeaux, France

For the ISBI HARDI reconstruction challenge 2013, we developed a local estimation method based on Multi-Tensor (MT) fitting with the Particle Swarm Optimization technique (PSO) [1]. We apply this reconstruction to the DTI and HARDI data categories.

To fit a MT to the diffusion signal $S = \{S_k\}_{k=0}^{M}$ with gradient scheme $\{b_k, g_k\}_{k=0}^{M}$ is to find some parameters so that $y = \{y_k\}_{k=0}^{M}$, $y_k = \sum_{i=0}^{N} f_i e^{-b_k g_k^t D_i g_k}$ resembles the measured signal S, where g_k is the kth normalized gradient wavevector and b_k the corresponding b-value, D_i is a rank 2 symmetric tensor with volume fraction f_i and N is the number of compartments in the fit.

To perform the MT fitting, we minimize the fitting error for some cost function, here the squared error between the measured signal and the MT approximation, $\|S-y\|_2^2$. This minimization is carried on by the particle swarm optimization. The PSO is a stochastic optimization algorithm using population interaction to find the minimum of a function $f : \mathbf{R}^n \to \mathbf{R}$. It starts by randomly initiating Np particles: points $\Omega_j^0 \in \mathbf{R}^n$, and Np velocities: points $v_j^1 \in \mathbf{R}^n$. These points then evolve into the search space according to $\Omega_j^{t+1} = \Omega_j^t + v_j^{t+1}$ and $v_j^{t+1} = wv_j^t + \phi_p r_p(p_j^t - \Omega_j^t) + \phi_g r_g(g^t - \Omega_j^t)$, where w, ϕ_p and ϕ_g are user tuned parameters, p_j^t is the j^{th} particle's best known position at iteration t, g^t is the swarm's best known position at iteration t and $r_p, r_g \sim \mathcal{U}[0,1]$. The process is repeated for Ni iterations or until some convergence criterion is met. The velocity update formula means that the particles are drawn to the swarm's best known position while being deflected by their own best location and conserving some of their past momentum. Particles near g will fully explore that area of the space and find the true local minimum while others will converge there from all over the space, allowing to potentially find new attractor points or finding a better value near their own best known location. Finally, the conservation of their previous velocity and its random weighting with p and g allow for the particles to escape non-optimal local minima, potentially attracting to them other particles that are trapped.

For the contest, we compared using the raw DW, the DW denoised with adaptive nonlocal means [2] using a rician noise model. As proposed in [3], each DW images were processed independently.

We constrained the MT model to use only prolate tensors and also tested adding an isotropic compartment and fixing the volume fraction to be equal between the non-isotropic compartments.

Since the number of compartments is a meta parameter, we chose as a strategy to overfit at every voxel by always estimating three fiber compartments and to re-estimate with less compartments certain voxels based on two criterion. We first enforce that no voxel has peaks closer to each other than θ°. This angular based pruning provides a good cleaning because the peaks tend to converge together when the voxel has been overmodeled. The only drawback is that we put a hard lower bound on the method's angular resolution. Secondly, we look at the model complexity of neighboring voxels after the angular pruning to detect outliers. A voxel that has more compartments than $\Psi\%$ of it's neighborhood is re-estimated with less compartments.

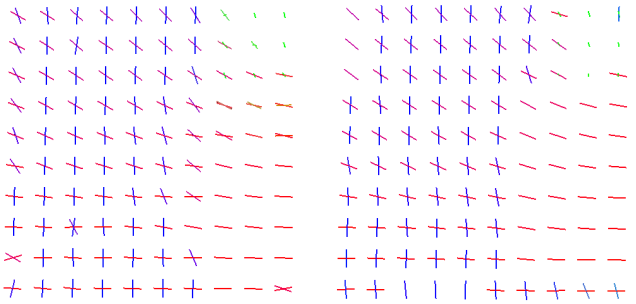

Fig. 1. Peaks in the testing dataset (ROI = [14:24, 22, 23:33]). Left is DTI, right is HARDI, both result on snr = 10 with denoising from [2].

In order to validate which denoising and MT constraints were optimal on the training data, we computed tractography for all the different combinations. Considering that the given ground truth was a binary connectivity matrices with given ROI, we generated connectivity matrix from track count and used them to qualitatively evaluate each method. For a specific threshold, we can binarize our matrix and obtain a connectivity error, # false connections + # missing connections. A false connection is two regions considered connected for that threshold that are not in the ground truth and a missing connection is two regions not considered connected for that threshold that are in the ground truth. Looking at that error for different thresholds gives an overview of the validity of the tractogram produced from that method. Indeed, a good tractogram should allow for a large range of threshold value that gives low connectivity error.

For the final result, for both the DTI dataset (32 directions at b = 1200 s/mm^2) and the HARDI dataset (64 directions at b = 3000 s/mm^2), we used the denoising from [2] for SNR 10 and 20 and no denoising for SNR 30. The MT model fitted had three prolate tensors and one isotropic tensor with fixed equal volume fractions. The pruning parameters were $\theta = 30^\circ$, $\Psi = 50\%$ for DTI and $\theta = 20^\circ$, $\Psi = 50\%$ for HARDI. We submitted the resulting peaks to the contest's organizers.

References

[1] J. Kennedy and R. C. Eberhart, "Particle swarm optimization," in *IEEE International Conference on Neural Networks*, vol. 4, pp. 1942 – 1948, 1995.

[2] J. V. Manjón, P. Coupé, L. Martí-Bonmatí, D. L. Collins, and M. Robles, "Adaptive non-local means denoising of mr images with spatially varying noise levels," *Journal of Magnetic Resonance Imaging*, vol. 31, no. 1, pp. 192–203, 2010.

[3] M. Descoteaux, N. Wiest-Daesslé, S. Prima, C. Barillot, and R. Deriche, "Impact of rician adapted non-local means filtering on hardi," in *Medical Image Computing and Computer-Assisted Intervention (MICCAI)*, vol. LNCS 5242, pp. 122–130, 2008.

Constrained spherical deconvolution on signal and ODF values

Eleftherios Garyfallidis*, Samuel St-Jean*, Michael Paquette*, Pierrick Coupé†, Maxime Descoteaux*
* Sherbrooke Connectivity Imaging Lab (SCIL), Computer Science department, Université de Sherbrooke, Sherbrooke, Canada
† CNRS, Laboratoire Bordelais de Recherche en Informatique, Bordeaux, France

For the purpose of the ISBI HARDI reconstruction challenge 2013 and for the categories DTI and HARDI acquisitions, we reconstructed the diffusion datasets using two well established methods: a) Spherical Deconvolution Transform (SDT) [1], [2] and b) Constrained Spherical Deconvolution (CSD) [3].

The SDT is a sharpening operation which transforms the smooth diffusion ODF into a sharper fiber ODF. The method is inspired by CSD [3] with, the main difference that the CSD is applied directly to the initial signal and the SDT directly to the ODF.

The idea here is that an ODF, for example the analytical Q-ball ODF ψ_{QBI}, can be formed by the convolution between the single fiber diffusion ODF kernel R and the true fiber ODF ψ_{SDT}.

$$\psi_{QBI}(\mathbf{u}) = \int_{|w|=1} R(\mathbf{u}\cdot\mathbf{w})\psi_{SDT}(\mathbf{w})dw \qquad (1)$$

Therefore, the deconvolution of ψ_{QBI} can recover a sharper ψ_{SDT}. We can derive the formula for the ψ_{SDT} using symmetrized spherical harmonics.

$$\psi_{SDT}(\mathbf{u}) = \sum_{j=1}^{R} 2\pi P_{l_j}(0)\frac{c_j}{f_j}Y_j(\mathbf{u}) \qquad (2)$$

For the derivation and explanation of the formula see [1].

The deconvolution that we used here is a fast converging iterative process. Usually, taking 5 to 10 iterations for convergence. The main choice to be considered both for SDT and CSD is the estimation of the single fiber response function R. We assume that R is derived from a prolate tensor. The eigenvalues of this tensor are estimated from the voxels with FA > 0.7. In Tab. 1 we show for the trainings sets that the estimated eigenvalues can change considerably (values scaled by 1000).

R estimation	DTI	HARDI
SNR 10	$\lambda_1 = 17.7$, $\lambda_2 = 4.1$	$\lambda_1 = 13.6$, $\lambda_2 = 3.8$
SNR 30	$\lambda_1 = 18.3$, $\lambda_2 = 3.7$	$\lambda_1 = 16.6$, $\lambda_2 = 3.8$

TABLE I

In order to deal with the high levels of noise, the diffusion weighted (DW) datasets for SNR 10 and 20 were denoised with the adaptive nonlocal means [4] using a rician noise model. As proposed in [5], each DW images were processed independently. The DW dataset with SNR 30 was left intact and no further denoising was performed.

In order to find the best parameters for the methods described here we created a connectivity matrix after generating deterministic streamlines from the ODFs of the training set. We finally selected the parameters which minimized the number of missing and false bundles in the training set and used those with the test data. In Fig.1 we see results from an ROI from slice Y=22 of the testing dataset reconstructed with CSD in A and C and with SDT in B and D. The

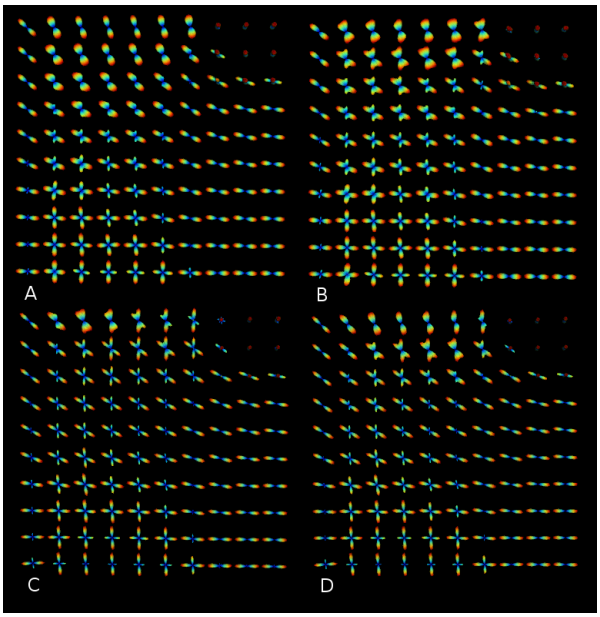

Fig. 1. ROI [14:24, 22, 23:33] of the denoised test dataset (SNR 10) provided by the organizers of the HARDI reconstruction challenge 2013. A) CSD DTI, B) SDT DTI, C) CSD HARDI, D) SDT HARDI.

spherical harmonic order used for the DTI datasests was 6 and for HARDI 8 both for CSD and SDT. In Fig. 1 we observe that SDT performed better in the DTI category but CSD performed slightly better the HARDI category as it managed to resolve more crossing fibers. For the challenge we submitted all results with ODFs saved as spherical harmonic coefficients of order 8. The source code for the methods described in this paper is available at dipy.org.

References

[1] M. Descoteaux, R. Deriche, T. R. Knösche, and A. Anwander, "Deterministic and probabilistic tractography based on complex fibre orientation distributions," *IEEE Transactions in Medical Imaging*, vol. 28, pp. 269–286, Febuary 2009.

[2] M. Descoteaux, *High Angular Resolution Diffusion MRI: from Local Estimation to Segmentation and Tractography*. PhD thesis, University of Nice-Sophia Antipolis, 2008.

[3] J.-D. Tournier, F. Calamante, and A. Connelly, "Robust determination of the fibre orientation distribution in diffusion mri: Non-negativity constrained super-resolved spherical deconvolution," *NeuroImage*, vol. 35, no. 4, pp. 1459–1472, 2007.

[4] J. V. Manjón, P. Coupé, L. Martí-Bonmatí, D. L. Collins, and M. Robles, "Adaptive non-local means denoising of mr images with spatially varying noise levels," *Journal of Magnetic Resonance Imaging*, vol. 31, no. 1, pp. 192–203, 2010.

[5] M. Descoteaux, N. Wiest-Daesslé, S. Prima, C. Barillot, and R. Deriche, "Impact of rician adapted non-local means filtering on hardi," in *Medical Image Computing and Computer-Assisted Intervention (MICCAI)*, vol. 5242, pp. 122–130, 2008.

Deconvolution enhanced Generalized Q-Sampling 2 and DSI deconvolution

Eleftherios Garyfallidis*, Michael Paquette*, Samuel St-Jean*, Pierrick Coupé†, Maxime Descoteaux*
* Sherbrooke Connectivity Imaging Lab (SCIL), Computer Science department, Université de Sherbrooke, Sherbrooke, Canada
† CNRS, Laboratoire Bordelais de Recherche en Informatique, Bordeaux, France

For the purpose of the ISBI HARDI reconstruction challenge 2013 and for the heavyweight category, we reconstructed the diffusion datasets using two methods: a) Generalized Q-sampling Imaging 2 [1], [2] with spherical deconvolution [3],[4] (GQID), and b) Diffusion Spectrum Imaging with Deconvolution [5] (DSID).

GQI2 provides a direct analytical formula to calculate the solid angle ODF (ψ_{GQI2}) of DSI without the need to first estimate the diffusion propagator:

$$\psi_{GQI2}(\mathbf{u}) = \lambda^3 \int S(\mathbf{q}) H(2\pi\lambda \mathbf{q}\cdot\mathbf{u}) d\mathbf{q} \qquad (1)$$

where $\mathbf{u}$ is the unit direction in the sphere, $\mathbf{q}$ is the q-space wave vector, S is the DW signal, λ is a smoothing parameter called the sampling length and

$$H(x) = \begin{cases} 2\cos(x)/x^2 + (x^2-2)\sin(x)/x^3, & x \neq 0 \\ 1/3 \qquad\qquad\qquad\qquad , & x = 0 \end{cases}$$

In [1], it was shown that ψ_{GQI2} creates ODFs with higher angular accuracy than standard DSI ODFs. In this work, we further extended ψ_{GQI2} with the spherical deconvolution transform (SDT).

The SDT is a sharpening operation which transforms the smooth diffusion ODF into a sharper fiber ODF [6]. The idea here is that an ODF for example the GQI2 ODF ψ_{GQI2} can be formed by convolution between the single fiber diffusion ODF kernel, R and the true fiber ODF ψ_{GQID}

$$\psi_{GQI2}(\mathbf{u}) = \int_{|w|=1} R(\mathbf{u}\cdot\mathbf{w}) \psi_{GQID}(\mathbf{w}) dw \qquad (2)$$

The deconvolution is a fast converging iterative process.

In order to deal with the high levels of noise, the diffusion weighted (DW) datasets for SNR 10 and 20 were denoised with adapted non-local means filtering [7] using a rician noise model. As proposed in [7], each DW images were processed independently.The DW dataset with SNR 30 was left intact and no further denoising was performed.

In GQI2, we usually use $2 \leq \lambda \leq 3$ as higher values can give noisier ODFs as we see at Fig.1Left. However, higher values of λ have the advantage that we are sampling from a higher radius in q-space (higher b-values) where most of the angular information lives. Using the GQID, we show at Fig.1Right that we can eliminate those noisy peaks and obtain sharper ODFs.

Apart from the GQID, for comparisons we also performed reconstructions using DSI with deconvolution [5]. This deconvolution is not a spherical one, but it is performed in the 3D grid of the DSI propagator using Lucy-Richardson deconvolution. DSID is known to create very sharp ODFs from last year's ISBI challenge.

In order to find the best parameters for the methods described here, we created a connectivity matrix after generating deterministic streamlines from the ODFs of the training set using the method provided by [8]. We finally selected the parameters which minimized the number of missing and false bundles in the training set and used those with the test datasets. For DSID we used a propagator grid of $35 \times 35 \times 35$. For GQID we used sampling length of $\lambda = 3.5$, SDT ratio of 0.22 and spherical harmonic order of 8. For the challenge we submitted all results with ODFs saved as spherical harmonic coefficients of order 8. The source code for the methods described in this paper is available at dipy.org.

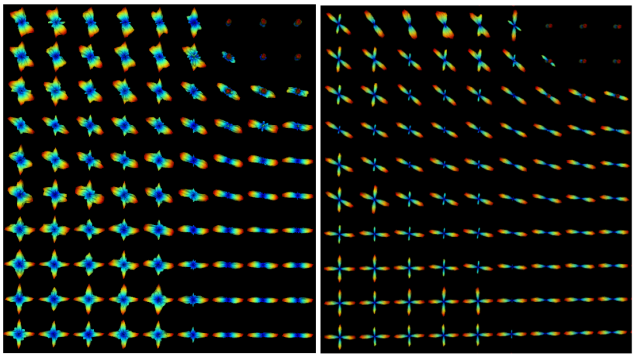

Fig. 1. A detail of slice Y=22 from the test data of the HARDI reconstruction challenge 2013 with GQI2 on the left and GQID ODFs on the right.

References

[1] E. Garyfallidis, *Towards an accurate brain tractography*. PhD thesis, University of Cambridge, 2012.

[2] F. Yeh, V. Wedeen, and W. Tseng, "Generalized Q-sampling imaging," *IEEE Transactions on Medical Imaging*, vol. 29, no. 9, pp. 1626–1635, 2010.

[3] M. Descoteaux, R. Deriche, T. R. Knösche, and A. Anwander, "Deterministic and probabilistic tractography based on complex fibre orientation distributions," *IEEE Transactions in Medical Imaging*, vol. 28, pp. 269–286, Febuary 2009.

[4] M. Descoteaux, *High Angular Resolution Diffusion MRI: from Local Estimation to Segmentation and Tractography*. PhD thesis, University of Nice-Sophia Antipolis, 2008.

[5] E. J. Canales-Rodríguez, Y. Iturria-Medina, Y. Aleman-Gomez, and L. Melie-Garcia, "Deconvolution in diffusion spectrum imaging," *NeuroImage*, vol. 50, no. 1, pp. 136–149, 2010.

[6] J.-D. Tournier, F. Calamante, and A. Connelly, "Robust determination of the fibre orientation distribution in diffusion mri: Non-negativity constrained super-resolved spherical deconvolution," *NeuroImage*, vol. 35, no. 4, pp. 1459–1472, 2007.

[7] M. Descoteaux, N. Wiest-Daesslé, S. Prima, C. Barillot, and R. Deriche, "Impact of rician adapted non-local means filtering on hardi," in *Medical Image Computing and Computer-Assisted Intervention (MICCAI)*, vol. 5242, pp. 122–130, 2008.

[8] G. Girard and M. Descoteaux, "Anatomical tissue probability priors for tractography," in *International Conference on Medical Image Computing and Computer Assisted Intervention (MICCAI'12) - Computational Diffusion MRI Workshop*, pp. 174–185, 2012.

Richardson-Lucy Spherical Deconvolution under Rician noise with Total Variation Spatial Regularization

Erick Jorge Canales-Rodríguez*†
* FIDMAG Research Foundation, Germanes Hospitalàries, (Barcelona, Spain)
† Centro de Investigación Biomédica en Red de Salud Mental (CIBERSAM), (Madrid, Spain)

Diffusion-MRI Reconstruction Challenge

Results presented at the "HARDI Reconstruction Challenge 2013" Workshop within the IEEE International Symposium on Biomedical Imaging (ISBI 2013). For more details see the contest website http://hardi.epfl.ch/static/events/2013_ISBI/.

Technical Description

Simulated Data

The phantom consisted in a set of different fiber bundles in a 3D image (matrix size: $50 \times 50 \times 50$), which "true" structure was not known in advance. For each voxel, the diffusion MRI signal has been generated using $N = 64$ sampling points on a sphere in q-space with a constant *b-value* equal to 3000 s/mm^2 (i.e., sampling class: **HARDI-LIKE**). The simulated signals were corrupted by Rician noise. Three datasets corresponding to different noise levels were provided by the organizers of the contest (i.e., signal-to-noise ratio *SNR* = 10, 20, 30).

Description of the Reconstruction Method

The spherical deconvolution method based on the Richardson-Lucy algorithm (RL) has demonstrated promising results in recovering the fiber orientation distribution from HARDI data [1], [2]. The aim of this work was to improve the original implementation of this method in two main aspects. The standard reconstruction is based on the assumption that the noise contaminating the signal follows a Gaussian distribution with mean value equal to zero. However, Rician noise introduces a signal-dependent bias into diffusion MRI measurements, which is particularly evident for low *SNR* values. As a result, the reconstructions assuming zero-mean Gaussian noise tend to produce small spurious fibers to explain this deviation from Gaussianity. In the original method this drawback was partially addressed by using a modified damped RL algorithm [1]. In contrast, in this work this problem is fully tackled by using the exact modeling of the Rician noise behaviour. In addition, in order to incorporate into the model prior knowledge about the underlying spatial structure of the fiber bundles (i.e., smooth structures with sharp edges), the maximum a posteriori solution is estimated using an expectation-maximization (EM) algorithm that includes a total variation (TV) spatial regularization term [3].

The derived algorithm in matrix-vector notation is:

$$\mathbf{f}_{k+1} = \mathbf{f}_k \times \frac{\mathbf{H}^T \left[\mathbf{S} \times \frac{I_1\left(\frac{\mathbf{S} \times \mathbf{H}\mathbf{f}_k}{\sigma^2}\right)}{I_0\left(\frac{\mathbf{S} \times \mathbf{H}\mathbf{f}_k}{\sigma^2}\right)} \right]}{\mathbf{H}^T \left(\mathbf{H}\mathbf{f}_k\right)} \times \mathbf{TV}_k, \qquad (1)$$

where I_0 and I_1 are the modified Bessel functions of the first kind of order zero and one, respectively; $\mathbf{f}_k$ is the estimated fiber orientation $(M \times 1)$ vector at iteration k at voxel (x, y, z); $\mathbf{S}$ is the HARDI sample signal $(N \times 1)$ vector at voxel (x, y, z); $\mathbf{H}$ is the dictionary of diffusion signals ($N \times M$ matrix); σ^2 is the variance of the noise and $\mathbf{TV}_k$ is the TV regularization $(M \times 1)$ vector at iteration k. The element at position i in this vector is computed as:

$$[\mathbf{TV}_k]_i = \frac{1}{1 - \lambda div\left(\frac{\nabla [\mathbf{f}_k]_i}{|\nabla [\mathbf{f}_k]_i|}\right)|_{(x,y,z)}}, \qquad (2)$$

where λ denotes the regularization parameter and $[\mathbf{f}_k]_i$ is a 3D image created by putting at each voxel the element at position i of their corresponding estimated fiber orientation vector. The intra-voxel variance is estimated similarly by maximum likelihood using the EM algorithm. At each iteration, the average variance σ_k^2 over all voxels is used to evaluate Eq.[1]. In the above equations, the multiplication "$\times$" and division operators are applied component-wise to the vector's elements.

Deconvolution was performed with the proposed algorithm using 300 iterations. The dictionary $\mathbf{H}$ was created imposing as fiber response a set of diffusion tensors with diffusivities equal to $[1.4, 0.4, 0.4] \times 10^{-3} mm^2/s$ and oriented along $M = 724$ spatial directions on the sphere. The dictionary also included two isotropic terms, to account for intra- (i.e., $0.2 \times 10^{-3} mm^2/s$) and extra-axonal diffusion (i.e., $1.4 \times 10^{-3} mm^2/s$). The starting condition for $\mathbf{f}_0$ was set as a non-negative iso-probable spherical function. The regularization parameter λ was adjusted adaptively at each iteration according to the discrepancy principle (i.e., it was selected to match the estimated variance σ_k^2).

This work is supported by FIDMAG and CIBERSAM

References

[1] Dell'acqua F., Scifo P., Rizzo G., Catani M., Simmons A., Scotti G., Fazio F., "A modified damped Richardson-Lucy algorithm to reduce isotropic background effects in spherical deconvolution", Neuroimage, 49(2), 1446-58 (2010).

[2] Parker G.D., Marshall D., Rosin P.L., Drage N., Richmond S., Jones D.K., "A pitfall in the reconstruction of fibre ODFs using spherical deconvolution of diffusion MRI data ", Neuroimage, 65, 433-48 (2013).

[3] Dey N., Blanc-Feraud L., Zimmer C., Roux P., Kam Z., Olivo-Marin J.C., Zerubia J.,"Richardson-Lucy algorithm with total variation regularization for 3D confocal microscope deconvolution", Microsc. Res. Tech., 69(4), 260-6 (2006).

High angular resolution diffusion MRI reconstruction through denoising and reweighted ℓ_1-minimization

Anna Auría*, Alessandro Daducci*, Jean-Philippe Thiran*† and Yves Wiaux *‡
* EPFL, École Polytechnique Fédérale de Lausanne, Switzerland
† University Hospital Center (CHUV) and University of Lausanne (UNIL), Switzerland
‡ Department of Radiology and Medical Informatics, University of Geneva (UniGE), Geneva, Switzerland

***Abstract*—Water diffusion in living tissues is highly affected by its cellular organization. In particular, water does not diffuse equally in all directions in highly ordered organs, such as the brain, and this property is useful to study the structure of spatial order in living tissues in a non-invasive way. A two-step optimization procedure is defined to reconstruct the intra-voxel structure in the context of the *HARDI reconstruction challenge (ISBI 2013)*. First, we perform a denoising of each 3D diffusion image at each q-space point sampled, exploiting the spatial gradient sparsity through convex optimization. Second, we assess the number and orientation of fibers in each voxel making use of an evolution of the reweighted sparse deconvolution approach formulated in [3].**

Spherical deconvolution approaches have become popular in the context of high angular resolution reconstruction of diffusion MRI since they allow to reconstruct the intra-voxel orientation of the fibers, the so-called fiber orientation distribution (FOD), with a relatively small number of samples. The FOD is a real-valued function on the sphere that indicates the orientation and the volume fraction of the fibers in a voxel and thus, it is a non-negative sparse function.

We can express the intra-voxel structure recovery problem in terms of the following linear formulation:

$$y = \Phi x + n, \tag{1}$$

where $x \in \mathbb{R}^n_+$ is the FOD, $y \in \mathbb{R}^m$ is the vector of measurements, Φ is the linear measurement operator and n is the acquisition noise.

In [3], the authors define a convex optimization problem for FOD reconstruction through a constrained formulation between sparsity prior and data, also making use of a reweighted sparse deconvolution. As a result, the following constrained ℓ_0 minimization problem can be written:

$$\min_{x \geq 0} \quad ||\Phi x - y||_2^2 \quad \text{s.t.} \quad ||x||_0 \leq k, \tag{2}$$

where $||\cdot||_0$ is the ℓ_0-norm and k indicates the expected number of fibers in a voxel. Like in [1], the sensing matrix or dictionary Φ is generated by applying a set of rotations to a given Gaussian kernel.

This formulation has been improved firstly by adding a pre-processing step, where the initial data have been denoised using a total variation prior by solving the following problem:

$$\min_{\bar{y} > 0} \quad ||\bar{y}||_{TV} \quad \text{s.t.} \quad ||y - \bar{y}||_2 < \epsilon. \tag{3}$$

In 3, y represents the data vector corresponding to one slice of the 3D volume, $\bar{y}$, its denoised version and $||\cdot||_{TV}$ stands for the total variation norm in 2D as defined in [5]. The ℓ_2 term is computed only for those voxels inside the region of interest. Assuming i.i.d. Gaussian noise with a variance estimated from voxels out of the region of the phantom, ϵ corresponds to a bound on a χ^2 distribution with as many degrees of freedom as the number of data samples. This pre-processing could be improved by solving the minimization problem globally, using the 3D TV-norm.

Secondly, we have observed that the final solution of 2 is sensitive to the parameter k chosen as an upper bound of the ℓ_0 norm, i.e. the maximum number of dictionary atoms that we allow to be active per voxel. Since we can expect to have at maximum $2-3$ fibers per voxel [4] and possibly some partial volume with grey matter or CSF, we have considered a $k_{max} = 5$. We solve the problem for $k \in \{1, .., k_{max}\}$ and we choose the solution $\hat{x}$ that minimizes the data term $||\Phi\hat{x} - y||_2^2$.

To extract the final fiber directions $\hat{x}$ and their volume fraction once we have recovered the sparse vector x, we perform a search for local maxima among all the directions within a cone of an angular resolution of 15°. As a final step, to refine each direction, we take into account the contributions of all neighboring directions within the same $15^\circ-$tolerance cone for each local maxima, performing a weighted sum of their directions. In all this process, we disregard the directions with contributions (i.e. coefficients) smaller than a fixed threshold that we have set to $\tau = 10^{-1}$.

For the *HARDI reconstruction challenge* (ISBI 2013), we have recovered the FOD from $m = 32$ data samples adquired with a DTI acquisition scheme and $b = 1200 s/mm^2$.

To generate a dictionary in the context of this contest, we estimate three different Gaussian kernels to model the diffusion signal in the regions of the brain corresponding to white matter, grey matter and CSF. Grey matter and CSF are typically isotropic media and the diffusion tensor is not sensitive to rotations. On the other hand, the kernel corresponding to the white matter is anisotropic. We estimate the singular values of the diffusion tensor from the data that we have available and subsequently we rotate it in 200 different directions equally distributed on the sphere. Therefore, the final number of atoms of the dictionary used for this reconstruction is $m \times n = 32 \times 202$ (200 atoms corresponding to white matter plus the two isotropic atoms corresponding to CSF and grey matter).

References

[1] B. Jian and B.C. Vemuri "A unified computational framework for deconvolution to reconstruct multiple fibers from diffusion weighted MRI", IEEE Trans Med Imaging, 26, 1464–1472 (2007).

[2] E. Candès, M. Wakin and S. Boyd "Enhancing sparsity by weighted ℓ_1 minimization", Journal of Fourier Analysis and Applications, 14, 877–905 (2008).

[3] A. Daducci, D. Van De Ville, J.P. Thiran and Y. Wiaux "Reweighted sparse deconvolution for high angular resolution diffusion MRI", pre-print in arXiv:1208.2247 (2012).

[4] B. Jeurissen, A. Leemans, D. Jones, J. Tournier, J. Sijbers, 2010 "Estimating the number of fiber orientations in diffusion MRI voxels : a constrained spherical deconvolution study", In: ISMRM. Stockholm (Sweden), p. 573 (2010).

[5] A. Chambolle, "An algorithm for total variation minimization and applications", Journal of Mathematical Imaging and Vision, 20, 1-2, 89-97 (2004).

Fiber structure assessment using FOD estimation followed by CP-decomposition

Yaniv Gur* and Chris R. Johnson*
* SCI Institute, University of Utah, 72 S. Central Campus Dr., SLC, UT 84112, USA

Introduction. The method we adopt here to extract the fiber structures is based on the algorithm proposed in [1]. It comprises two steps: First, a fiber orientation distribution (FOD) is fitted to the DWI measurements using a spherical deconvolution operation. Second, the FOD, represented as a higher-order tensor, is decomposed into rank-one tensors by means of the CP-decomposition. The tensor decomposition provides information on fiber orientations, volume fractions, and number of fiber compartments in the voxel.

Method. Given diffusion weighted measurements in n directions for a single b-value, $\{S(\mathbf{g}_i, b)\}_{i=1}^n$, to estimate the FOD we aim to solve the following problem:

$$\min_F \frac{1}{2}\sum_{i=1}^{n}\left\| S(\mathbf{g}_i,b) - S_0\int_{S^2} F(\mathbf{v})K(\mathbf{g}_i,\mathbf{v},b)d\mathbf{v}\right\|^2 \quad (1)$$

subject to

$$F(\mathbf{w}_i)\geq 0, \quad \mathbf{w}_1,\ldots,\mathbf{w}_N \in S^2,$$

where K is a single fiber response kernel, which is chosen here as the bipolar Watson distribution: $K(\mathbf{g}\cdot\mathbf{v},b) = e^{-\delta(\mathbf{g}^T\mathbf{v})^2}$. This estimation problem is solved under a set of constraints that guarantee the non-negativity of the FOD at a discrete set of directions (the N directions used to represent the FOD). Following [2], the FOD is represented here as a spherical, even-order homogeneous polynomial induced by a symmetric higher-order tensor.

This problem can be solved for homogenous polynomials of any order, as long as the number of measurements is larger than the number of polynomial coefficients. In this challenge, we only consider fourth-order tensors, since at orders higher than four the impact of noise becomes more dominant, and affects the estimation accuracy. A symmetric fourth-order tensor has 15 unique coefficients associated with a homogeneous polynomial:

$$F(\mathbf{g}) = \sum_{a=0}^{4}\sum_{b=0}^{4-a} c_{ab} g_1^a g_2^b g_3^{4-a-b}, \quad (2)$$

where c_{ab} denote the unique tensor coefficients and g_1, g_2 and g_3 are the components of the gradient direction $\mathbf{g}$. The tensor coefficients are estimated by solving (1). In terms of this FOD representation, the "clean" diffusion signal at directions $\mathbf{g}$ is described as follows:

$$S(\mathbf{g},b) = \sum_{a=0}^{4}\sum_{b=0}^{4-a} c_{ab}\int_{\mathbf{v}\in S^2} v_1^a v_2^b v_3^{4-a-b} K(\mathbf{g},\mathbf{v},b)d\mathbf{v}. \quad (3)$$

The integrations in this expression cannot be done analytically, hence, the integrals here are approximated numerically.

The optimization problem (1) can be formulated in matrix form. We first define a matrix, C, whose entries correspond to the numerical approximation of (3) for each monomial, in each direction $\mathbf{g}_i$. The size of this matrix is then $n \times m$ where n is the number of gradient directions, and m is the number of unique tensor coefficients. The linear constraints that impose the positivity on F are then arranged in a $N \times m$ matrix A. Each row of A corresponds to a different direction, and each column corresponds to a different monomial. The multiplication $\mathrm{A}\mathbf{x}$ results in a N-dimensional vector that defines a set of N linear constraints, and each element of this vector corresponds to $F(\mathbf{w}_i)$.

Finally, using the matrix notations defined above, the following problem is solved for each voxel:

$$\arg\min_{\mathbf{x}} \frac{1}{2}\left\|\mathbf{S} - \mathbf{C}\cdot\mathbf{x}\right\|^2 \quad \text{subject to} \quad -\mathrm{A}\mathbf{x} \leq \mathbf{b}, \quad (4)$$

where $\mathbf{S}$ is the DW measurements vector, and $\mathbf{b}$ is a N-dimensional vector which defines the boundary of the convex polytope on which we minimize the objective function. Setting the values of $\mathbf{b}$ to zero, results in estimation of a non-negative FOD in N discrete directions. We solve this problem using the convex optimization toolbox (CVX) [3]. Given the optimal vector of coefficients, $\mathbf{x}^\star$, the FOD is computed by $F = \mathrm{A}\mathbf{x}^\star$. The unique tensor coefficients are then arranged in a fourth-order tensor using the symmetry, and the appropriate monomial factors.

Once the FOD has been estimated we proceed to extracting the fiber directions and fractions. To that end, we approximate the tensor using rank-one tensors by means of the CP-decomposition such that:

$$\mathcal{D} \approx \sum_{r=1}^{k} \lambda_r \mathbf{v}_r^1 \otimes \mathbf{v}_r^2 \otimes \cdots \otimes \mathbf{v}_r^n, \quad (5)$$

where $\mathbf{v}$ are first-order tensors (vectors), and n is the order of the tensor. In our case $n = 4$ and $\mathbf{v} \in \mathrm{R}^3$. Since $\mathcal{D}$ is symmetric here, $\mathbf{v}_r^1 = \mathbf{v}_r^2 = \ldots = \mathbf{v}_r^n$. Finally, the parameter k corresponds to the number of fiber compartments, $\mathbf{v}_r$ correspond to the fiber orientations, and λ_i to the fiber fractions (after normalization). To select the number of fiber compartments in each voxel, we first decompose the estimated tensor into $k = 3$ rank-one terms. Then, we normalize the weights λ_r's such that their sum is one. Finally, we keep only the terms which their weight is above a certain threshold. We applied two different thresholds, the first is for transition from one to two fibers, and the second is for transition from two to three fibers. These thresholds were separately set for every SNR based on the training data. The kernel parameter was set to $\delta = 200$ for the three different SNR datasets.

This work is supported in part by NIH grants 5P41RR012553-14 and 8P41GM103545-14.

REFERENCES

[1] Fangxiang Jiao, Yaniv Gur, Chris R. Johnson, and Sarang Joshi, "Detection of crossing white matter fibers with high-order tensors and rank-k decompositions," in *IPMI'11*, 2011, vol. 6801 of *LNCS*, pp. 538–549.

[2] Yonas Weldeselassie, Angelos Barmpoutis, and M. Stella Atkins, "Symmetric positive-definite cartesian tensor orientation distribution functions (CT-ODF)," in *MICCAI'10*, 2010, vol. 6361 of *LNCS*, pp. 582–589.

[3] M. Grant and S. Boyd, "CVX: Matlab software for disciplined convex programming, version 1.21," http://cvxr.com/cvx, Oct. 2010.

A Direct Approach for ODF Estimation using Symmetric Tensor Decomposition

Yaniv Gur* and Chris R. Johnson*
* SCI Institute, University of Utah, 72 S. Central Campus Dr., SLC, UT 84112, USA

Introduction. The majority of HARDI reconstruction techniques use an ODF to delineate the diffusion pattern within a brain voxel. The dominant diffusion directions (i.e., the fiber orientations) are extracted from the ODF using various techniques (e.g., [1]). In many cases the complexity of these techniques is high and their accuracy is limited by the quality of the ODF reconstruction. To overcome these limitations, we suggest here to reconstruct the fiber orientations and the volume fractions *directly* from the HARDI measurements, without estimating an ODF. The proposed approach relies on the spherical deconvolution technique and decomposition of homogenous polynomials by means of powers of linear-forms [2], which is known as a *symmetric tensor decomposition*. An ODF is directly related to a homogenous polynomial or a higher-order tensor [3], therefore, it could be decomposed similarly. Since an ODF encodes information on dominant diffusion directions as well as noise, to recover the dominant diffusion directions only we propose to use a lower-rank approximation of the ODF by means of power of linear-forms. In this formulation, each linear-form represent a single fiber and convolved to a single-fiber response kernel. This leads to a spherical deconvolution problem which is solved here using an iterative alternating algorithm which is based on the Levenberg-Marquardt technique. The method we use here is described in detail in [4].

Method. Spherical deconvolution is a common technique to recover major diffusion directions from DWI data [5]. It is based on a convolution between a spherically symmetric function, known as fODF, and an axially symmetric kernel that represents a single fiber response. Given a vector of n DWI measurements in the gradient directions, the fODF, denoted by F, is reconstructed by solving the following deconvolution problem:

$$\min_{F} \frac{1}{2} \sum_{i=1}^{n} \left\| S(\mathbf{g}_i, b) - S_0 \int_{S^2} F(\mathbf{v}) K(\mathbf{g}_i, \mathbf{v}) d\mathbf{v} \right\|^2 . \qquad (1)$$

This problem is solved for a fixed kernel, K, where its width is adjusted to the particular dataset. The resulting fODF represents a sum of spherical delta functions aligned with the fiber orientations and weighted by the volume fractions.

To combine the fODF reconstruction and the orientations estimation into one optimization problem, we first approximate the fODF using a lower-rank approximation by means of polynomial approximation (symmetric tensor decomposition) such that:

$$F(\mathbf{v}) \sim \sum_{i=1}^{\tilde{r}} \gamma_i f_i^d = \sum_{i=1}^{\tilde{r}} (\boldsymbol{\alpha}_i \cdot \mathbf{v})^d, \quad \tilde{r} < r, \qquad (2)$$

where $\boldsymbol{\alpha}_i \in \mathbb{R}^3$, $\mathbf{v} \in S^2$ and each fiber aligned in direction $\boldsymbol{\alpha}_i$ is identified with a linear form $(\boldsymbol{\alpha}_i \cdot \mathbf{v})^d$. The number of fibers to be reconstructed is determined by the approximation rank $\tilde{r}$ and the expansion coefficients are defined as $\gamma_i = \|\boldsymbol{\alpha}_i\|^d$.

Next, we substitute (2) into (1). This leads to the following non-linear optimization problem:

$$\min_{\boldsymbol{\alpha}_j} \frac{1}{2} \sum_{i=1}^{n} \left\| S(\mathbf{g}_i, b) - S_0 \int_{S^2} \sum_{j=1}^{\tilde{r}} (\boldsymbol{\alpha}_j \cdot \mathbf{v})^d K(\mathbf{g}_i, \mathbf{v}) d\mathbf{v} \right\|^2 . \qquad (3)$$

This problem is solved for the coefficients of the linear-forms(three coefficients per fiber) which are directly estimated from the DWI measurements. The fiber orientations and the volume fractions are derived as follows: Since each linear-form gets its maximum at the direction specified by $\boldsymbol{\alpha}_j$, given the optimal solution, $\tilde{\boldsymbol{\alpha}}_j$, the corresponding fiber orientation is simply $\mathbf{u}_j = \frac{\tilde{\boldsymbol{\alpha}}_j}{\|\tilde{\boldsymbol{\alpha}}_j\|}$. As we do not impose the constraint $\sum_{j=1}^{\tilde{r}} \|\boldsymbol{\alpha}_j\|^d = 1$, the corresponding volume fraction is given by $w_j = \frac{\|\tilde{\boldsymbol{\alpha}}_j\|^d}{\sum_{j=1}^{\tilde{r}} \|\tilde{\boldsymbol{\alpha}}_j\|^d}$.

The problem (3) is non-linear and we solve it here by means of the the Levenberg-Marquart (LM) optimization method. Using this method, we first reconstruct one fiber ($\tilde{r} = 1$). Then, we increment $\tilde{r} = 1$ by one and reconstruct two fibers. The solution for ($\tilde{r} = 2$) is accepted if the condition $w_2 > t_1$ holds, where w_2 is the lowest volume fraction and t_1 is a predefined threshold. If the condition holds, the rank is incremented again and three fibers are reconstructed. Otherwise, the single fiber model is selected. Similarly, the three fibers model is accepted if $w_2 > t_2$. In each case, when the rank is incremented, the solutions of the lower rank problem are used for initialization. The thresholds t_1 and t_2 were adjusted based on the training data and their values depend on the SNR.

This work is supported in part by NIH grants 5P41RR012553-14 and 8P41GM103545-14.

REFERENCES

[1] I. Aganj, C. Lenglet, and G. Sapiro, "ODF maxima extraction in spherical harmonic representation via analytical search space reduction," in *MICCAI'10*, 2010, vol. 6361 of *LNCS*, pp. 84–91.

[2] Jérôme Brachat, Pierre Comon, Bernard Mourrain, and Elias P. Tsigaridas, "Symmetric tensor decomposition," *Linear Algebra and Applications*, vol. 433, no. 11-12, pp. 1851–1872, 2010.

[3] Maxime Descoteaux, Elaine Angelino, Shaun Fitzgibbons, and Rachid Deriche, "Apparent diffusion coefficients from high angular resolution diffusion imaging: Estimation and applications," *Magnetic Resonance in Medicine*, vol. 56, no. 2, pp. 395–410, 2006.

[4] Yaniv Gur, Fangxiang Jiao, Stella X. Zhu, and Chris R. Johnson, "White matter structure assessment from reduced hardi data using low-rank polynomial approximations," in *MICCAI 2012 Workshop on Computational Diffusion MRI (CDMRI 2012)*, October 2012, pp. 186–197.

[5] J-Donald Tournier, Fernando Calamante, and Alan Connelly, "Robust determination of the fibre orientation distribution in diffusion MRI: Non-negativity constrained super-resolved spherical deconvolution," *NeuroImage*, vol. 35, no. 4, pp. 1459–1472, 2007.

Non-Local Non-Negative Spherical Deconvolution for Single and Multiple Shell Diffusion MRI

Jian Cheng*, Rachid Deriche†, Tianzi Jiang‡, Dinggang Shen*, and Pew-Thian Yap*
* Univerisity of North Carolina at Chapel Hill
† INRIA Sophia Antipolis
‡ Institute of Automation, Chinese Academy of Sciences

I. Introduction

In diffusion MRI (dMRI), Spherical Deconvolution (SD) is a category of methods which estimate the fiber Orientation Distribution Function (fODF). Existing SD methods, including the widely used Constrained SD [1], normally have two common limitations: 1) the non-negativity constraint of the fODFs is not satisfied in the continuous sphere; 2) many spurious peaks are detected, especially in the regions with low anisotropy; In [2], we proposed a novel SD method, called Non-Negative SD (NNSD), to avoid these two limitations. NNSD guarantees the non-negativity constraint of fODFs in the continuous sphere $\mathbb{S}^2$, and it is robust to the false positive peaks. In this abstract, we propose Non-Local NNSD (NLNNSD) which considers non-local spatial information and Rician noise in NNSD, and apply it to the testing data in ISBI contest.

II. Method

We represent the square root of fODF $\Phi(\mathbf{u})$ as a linear combination of real Spherical Harmonic (SH) basis $Y_l^m(\mathbf{u})$ with even order, i.e. $\Phi(\mathbf{u}) = \left(\sum_{l=0}^{L}\sum_{m=-l}^{l} c_{lm}Y_l^m(\mathbf{u})\right)^2 = \sum_{\alpha=0}^{2L}\sum_{\beta=-\alpha}^{\alpha}\left(\sum_{l,m}^{L}\sum_{l',m'}^{L} c_{lm}c_{l'm'}Q_{ll'\alpha}^{mm'\beta}\right)Y_\alpha^\beta(\mathbf{u})$, where $\mathbf{u}\in\mathbb{S}^2$, $Q_{ll'\alpha}^{mm'\beta} = \int_{\mathbb{S}^2} Y_l^m(\mathbf{u})Y_{l'}^{m'}(\mathbf{u})Y_\alpha^\beta(\mathbf{u})d\mathbf{u}$ is the integral constant of three SHs which can be calculated from the Wigner 3-j symbol. Then based on the closed form of spherical convolution using SH basis, for a given axisymmetric fiber response function along z-axis $H(q\mathbf{u}|(0,0,1)) = \sum_{l=0}^{L} h_l(q)Y_l^0(\mathbf{u})$, the convolved diffusion signal is

$$E(q\mathbf{u}) = \sum_{\alpha=0}^{2L}\sum_{\beta=-\alpha}^{\alpha}\sum_{l,m}^{L}\sum_{l',m'}^{L}\sqrt{\frac{4\pi}{2\alpha+1}}c_{lm}c_{l'm'}Q_{ll'\alpha}^{mm'\beta}h_\alpha(q)Y_\alpha^\beta(\mathbf{u}) = \boldsymbol{c}^T\mathbf{K}(q\mathbf{u})\boldsymbol{c} \quad (1)$$

where for any fixed vector $\mathbf{q} = q\mathbf{u}$, $\mathbf{K}(\mathbf{u})$ is a square matrix with the elements $\mathbf{K}_{ll'}^{mm'}(q\mathbf{u}) = \sum_{\alpha=0}^{2L}\sum_{\beta=-\alpha}^{\alpha}\sqrt{\frac{4\pi}{2\alpha+1}}Q_{ll'\alpha}^{mm'\beta}h_\alpha(q)Y_\alpha^\beta(\mathbf{u})$. Then NNSD [2] is to estimate $\boldsymbol{c}$ by minimizing

$$J(\boldsymbol{c}) = \frac{1}{2}\sum_{i=1}^{N}\left(\boldsymbol{c}^T\mathbf{K}(q\mathbf{u})\boldsymbol{c} - E_i\right)^2 + \frac{1}{2}\boldsymbol{c}^T\Lambda\boldsymbol{c}, \qquad \text{s.t.}\ \ \|\boldsymbol{c}\| = 1 \quad (2)$$

where Λ is a diagonal matrix with elements $\Lambda_{lm} = \lambda_{NNSD}l^2(l+1)^2$ for the Laplace-Beltrami regularization. The constraint $\|\boldsymbol{c}\| = 1$ is because of $\int_{\mathbb{S}^2}\Phi(\mathbf{u})d\mathbf{u} = 1$. In this abstract, we propose Non-local NNSD (NLNNSD) which considers the non-local spatial information and Rician noise. Non-local mean has been used in image denoise [3], [4] and regularization [5]. The cost function in NLNNSD is

$$J(\{\boldsymbol{c}^x\}) = \frac{1}{2}\sum_{x=1}^{V}\sum_{i=1}^{N}\left((\boldsymbol{c}^x)^T\mathbf{K}(q\mathbf{u})\boldsymbol{c}^x - \mathrm{NLM}(E_i^x)\right)^2 + \frac{1}{2}(\boldsymbol{c}^x)^T\Lambda\boldsymbol{c}^x + \frac{1}{2}\lambda_{NLM}\|\boldsymbol{c}^x - \mathrm{NLM}(\boldsymbol{c}^x)\|^2 \quad (3)$$

where $\boldsymbol{c}^x$ and E_i^x are the coefficient vector and diffusion signal at voxel x, V is the number of voxels, $\mathrm{NLM}(\boldsymbol{c}^x) = \arg\min_{\boldsymbol{c}}\sum_{y\in V} w_y d(\boldsymbol{c},\boldsymbol{c}^y)^2$ is the non-local Riemannian mean of $\boldsymbol{c}^x$ [6], $\mathrm{NLM}(E_i^x) = \sqrt{\sum_{y\in V} p_y (E_i^y)^2 - 2\sigma^2}$ is the non-local mean of E_i^x considering Rician noise with standard deviation of σ. w_y is the non-local weights determined by the distance of coefficient vectors, i.e. $w_y = \frac{1}{Z_y}\exp(-\frac{\sum_{j\in N_x,k\in N_y} G_a\|\boldsymbol{c}^j-\boldsymbol{c}^k\|^2}{2h^2})$, where $\boldsymbol{c}^j$ and $\boldsymbol{c}^k$ are the coefficient vectors respectively in the neighborhood N_x of x and the neighborhood N_y of y, G_a is the Gaussian weighting with standard deviation of a, and Z_y is the normalization factor. p_y is the non-local weight determined by the distance of $\{E_i^x\}$ with another set of $\{a,h\}$.

To minimize Eq. (3) with the constraint $\|\boldsymbol{c}\| = 1$, we first set $\lambda_{NLM} = 0$, and perform a Riemannian gradient descent on the sphere $\|\boldsymbol{c}\| = 1$ [6] to minimize $J(\boldsymbol{c}^x)$ individually for each voxel x.

$$(\boldsymbol{c}^x)^{(k+1)} = \mathrm{Exp}_{(\boldsymbol{c}^x)(k)}\left(-dt\frac{\nabla J(\boldsymbol{c}^x)}{\|\nabla J(\boldsymbol{c}^x)\|}\right), \quad \mathrm{Exp}_{\boldsymbol{c}}(\boldsymbol{v}) = \boldsymbol{c}\cos\|\boldsymbol{v}\| + \frac{\boldsymbol{v}}{\|\boldsymbol{v}\|}\sin\|\boldsymbol{v}\|$$

The isotropic fODF with $\boldsymbol{c} = (1,0,\ldots,0)^T$ is chosen as the initialization. Then the non-local Riemannian mean is performed to calculate $\mathrm{NLM}(\boldsymbol{c}^x)$ at each voxel. Then the Riemannian gradient descent is performed again with λ_{NLM} and the estimated non-local mean $\mathrm{NLM}(\boldsymbol{c}^x)$ in Eq. (3). Note that this procedure can be iteratively performed to update $\mathrm{NLM}(\boldsymbol{c}^x)$ and $\boldsymbol{c}^x$, however in practice we found the result with just one iteration is enough.

III. ISBI HARDI Reconstruction Challenge

In the ISBI reconstruction challenge, the testing data was generated based on Numerical Fibre Generation toolbox [7]. we test the proposed NLNNSD in the data with three kind of sampling schemes: 1) single shell DTI scheme with 32 directions, $b = 1200s/mm^2$; 2) single shell HARDI scheme with 64 directions, $b = 3000s/mm^2$; 3) multiple shell DSI-like scheme with 514 directions, $b\in(0,4000]s/mm^2$. For all night datasets (three schemes with three SNR 10, 20, 30), we fixed $L = 8$, $\lambda_{NNSD} = 0$, $\lambda_{NLM} = 1$, and used the tensor fiber response function with FA of 0.8, mean diffusivity of 0.8. In the non-local mean of $\boldsymbol{c}^x$ and E_i^x, we uses a $11\times11\times11$ search window, and a $3\times3\times3$ patch to define the weights, where the parameters a and h were tuned respectively for $\{\boldsymbol{c}^x\}$ and $\{E_i^x\}$ to obtain visually good results for each dataset.

References

[1] J. Tournier, F. Calamante, A. Connelly, "Robust determination of the fibre orientation distribution in diffusion MRI: non-negativity constrained super-resolved spherical deconvolution", NeuroImage 35(4) 1459–1472 (2007).
[2] J. Cheng, D. Shen, P.-T. Yap, "Non-Negative Spherical Deconvolution for Fiber Orientation Distribution Estimation", ISMRM (2013).
[3] A. Buades, B. Coll. J.M. Morel, "A non-local algorithm for image denoising" CVPR (2005).
[4] M. Descoteaux, N. Wiest-Daessle, S. Prima, C. Barillot, R. Deriche, "Impact of Rician Adapted Non-local Means Filtering on HARDI", MICCAI (2008).
[5] G. Peyré, S. Bougleux, L. Cohen, "Non-local regularization of inverse problems", ECCV, 2008.
[6] J. Cheng, A. Ghosh,T. Jiang, R. Deriche, "A Riemannian Framework for Orientation Distribution Function Computing", MICCAI (2009).
[7] T. Close, J. Tournier, F. Calamante, L. Johnston, I. Mareels, A. Connelly, "A software tool to generate simulated white matter structures for the assessment of fibre-tracking algorithms", NeuroImage (2009).

Contextual Enhancements on DW-MRI

R.H.J. Fick*†, R. Duits*, E.J. Creusen*, T.C.J. Dela Haije*, P.P.W. Ossenblok†, B.M. ter Haar Romenij* and A. Vilanova*
* Eindhoven University of Technology, The Netherlands
† Kempenhaeghe Center for Epilepsy, The Netherlands

I. Introduction

Constrained Spherical Deconvolution (CSD) [1] is a popular technique for estimating Fiber Orientation Density functions (FODs) directly from Diffusion Weighted MRI (DW-MRI) data. In our approach we use nonlinear contextual enhancements [2], [3], [4] to further process the results of the CSD algorithm. This method denoises the FOD field while enhancing aligned glyphs, and was shown to improve extraction of complex angular structures even from low angular resolution data such as obtained from DTI acquisition schemes [5]. In this challenge we use this approach in both the DTI and HARDI categories.

II. Methods

We use CSD to obtain FODs from the raw data. CSD uses a non-negativity constraint which counters the ill-posedness of spherical deconvolution. The algorithm iteratively improves an initial estimate of the FOD, given by a spherical deconvolution with a kernel estimated from the data.

Enhancement of the FODs is performed using a framework presented by Duits et al. [2] that is based on the coupling of positions and orientations. This coupling induces a (left-invariant) moving frame of reference $\{\mathcal{A}_i\}_{i=1}^5$ consisting of tangent vectors $\mathcal{A}_i$, which can be regarded as differential operators. Figure 1 shows a schematic representation of these tangent vectors. In terms of this moving frame, the (nonlinearly) enhanced field of FODs W can be expressed as the solution to the diffusion equation

$$\begin{cases} \partial_t W(\mathbf{y},\mathbf{n};t) = \left(\mathcal{A}_3 \tilde{D}^{33} \mathcal{A}_3 + D^{44}\left((\mathcal{A}_4)^2 + (\mathcal{A}_5)^2\right)\right) W(\mathbf{y},\mathbf{n};t) \\ W(\mathbf{y},\mathbf{n};0) = U(\mathbf{y},\mathbf{n}) \end{cases}$$

Here the adaptive diffusivity function $\tilde{D}^{33}$ is given by $\tilde{D}^{33}(\mathbf{y},\mathbf{n}) = D^{33} e^{-\frac{(\mathcal{A}_3 W(\mathbf{y},\mathbf{n};t))^2}{K^2}}$, where K is the anisotropic diffusion parameter typically estimated [3] from $\left\{|(\mathcal{A}_3 U)(\mathbf{y},\mathbf{n})| \,|\, \mathbf{y}\in\mathbb{R}^3, \mathbf{n}\in S^2\right\}$. The parameters D^{33} and D^{44} are used to balance the spatial and angular effects of the operator, and the initial condition U is given by the FOD field obtained from CSD.

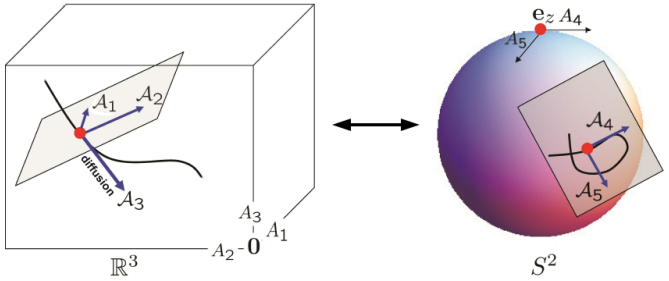

Fig. 1: Visualization of the coupling between position and orientation, which follows from the non-commutative relation between translation and rotation, note that $\mathcal{A}_i|_e = A_i$ and $\mathcal{A}_i|_g = (L_g)_* A_i$.

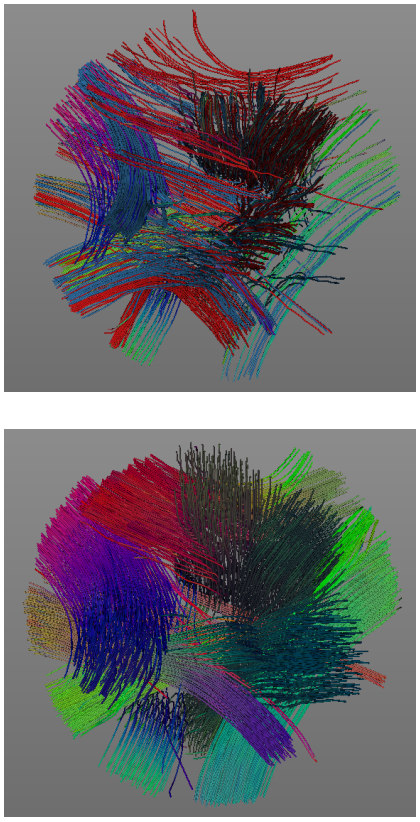

Fig. 2: Streamline tractography results on the training data set with SNR 10. Top: CSD. Bottom: Enhanced CSD.

III. Parameter Settings

For the DTI category we used a maximum spherical harmonics order $l_{\max} = 6$, $D^{44} = 0.003$ and $K = 0.06$. For the HARDI category we used $l_{\max} = 8$, and $D^{44} = 0.005$ and $K = 0.1$. For both categories we had $D^{33} = 1$, and $t = 3$. The enhancements used a tenth order tessellation of the icosahedron to discretize S^2.

IV. Preliminary Results

Figure 2 shows processed data from the DTI category before and after enhancements.

References

[1] J. Tournier, F. Calamante, and A. Connelly, "Robust Determination of the Fibre Orientation Distribution in Diffusion MRI: Non-negativity Constrained Super-esolved Spherical Deconvolution", NeuroImage, Volume 35, Pages 1459—1472 (2007).
[2] R. Duits and E. Franken, "Left-Invariant Diffusions on the Space of Positions and Orientations and their Application to Crossing-Preserving Smoothing of HARDI images", IJCV, Volume 92 Issue 3, Pages 231-264 (2011).
[3] E. Creusen, R. Duits, A. Vilanova and L. Florack, "Numerical Schemes for Linear and Non-Linear Enhancement of DW-MRI", NM-TMA, 6(1), 138-168 (2013).
[4] R. Duits, T. Dela Haije, E. Creusen, A. Gosh, "Morphological and Linear Scale Spaces for Fiber Enhancement in DW-MRI", JMIV, (2013).
[5] Prckovska et al., "Extrapolating Fiber Crossings From DTI Data: Can We Infer Similar Fiber Crossings as in HARDI?", MICCAI, 1-10 (2010).

Periodic Spherical Spiral Sampling in Gradient Direction Domain Improves Diffusion MRI Accuracy

Farshid Sepehrband[1], Jeiran Choupan[1], Yaniv Gal[2], David C Reuten[1], and Zhengyi Yang[2]
[1]Centre for Advanced Imaging, The University of Queensland, Brisbane, Australia
[2]School of Information Technology and Electrical Engineering, The University of Queensland, Brisbane, Australia
Email: f.sepehrband@uq.edu.au

I. Introduction

Diffusion-Weighted Imaging (DWI) is affected by measurement errors from a number of sources, reducing the accuracy of its applications such as tractography [1]. Many methods have been proposed to improve DWI data quality [2]. Existing sampling schemes use uniformly distributed gradient directions over the sphere and data smoothing is often carried out in image domain or k-space [2]-[5]. To exploit the continuity of the diffusion signal in the 'gradient direction domain' for voxelwise smoothing, we propose a new sampling scheme based on periodic spherical spiral sampling with constant angular velocity. The acquired diffusion-weighted signal in each voxel inherits the sampling periodicity, having noise mainly concentrated in high frequencies. Characteristics of this one-dimensional periodic signal were investigated and employed as features to distinguish background voxels from those containing fibres.

II. Method

Periodic spherical spiral sampling: Sampling coordinates of gradient directions are obtained using following equation:

$$\mathbf{d}_i = \begin{bmatrix} x_i & y_i & z_i \end{bmatrix} = \begin{bmatrix} \sin(\Theta_i)\cos(\Phi_i) & \sin(\Theta_i)\sin(\Phi_i) & \cos(\Phi_i) \end{bmatrix}$$

$$\Theta_i = ir/2\pi \quad \Phi_i = ir \quad i = 0,1,...,N$$

where, r is the angular velocity and N is the total number of samples. In order to cover half of spherical coordinates, $N = (n_p/2)^2$, where n_p is the number of samples in each period. Acquired diffusion-weighted signal $\mathbf{S}$ in a voxel is:

$$\mathbf{S} = E(b,\mathbf{d}_i)/E0, \quad b = (\Delta - \delta/3)(\delta\gamma|G|)^2$$

where E is diffusion-weighted signal, b is the b-value, $E0$ is diffusion-weighted signal for a b-value of zero.

Denoising: The acquired diffusion-weighted signal sequence in each voxel ($\mathbf{S}$) in the 'gradient direction domain' was first de-trended by subtracting its least squares linear fit Denoising was then achieved by low-pass filtering. The linear trend of the sequence was then restored. A fixed cut-off frequency is used for all the voxels.

Synthetic data: We generated two datasets with different numbers of samples and b-values. The first dataset was simulated using 226 samples with 12° angular velocity and b-value = 2,000 s/mm^2, plus one measurement with b-value equal to zero. The second dataset was simulated using 26 samples with 36° angular velocity and b-value of 1,200 s/mm^2, plus one measurement with b-value equal to zero. The simulated data were provided by the organizer of the high angular resolution diffusion MRI reconstruction challenge (http://hardi.epfl.ch/static/events/2013_ISBI/).

Data analysis: Data analysis was undertaken using in-house software written in MATLAB® (MathWorks, Natick, MA) and MRtrix [6]. We first denoised both datasets using a cut-off frequency of 28 and 6, respectively. For the dataset with 26 samples, the signal was interpolated using Fourier expansion, resulting in 200 samples. Voxels were classified into four classes: background voxels, isotropic diffusion voxels, fibre bundles, and boundaries. A threshold-based decision tree algorithm using features extracted from the signal sequences was used to perform the classification. The features used include Mean Signal Attenuation (MSA) and Fluctuation Rate (FR), the difference between maximum and minimum diffusion signal values. Voxels lying between fibre bundles and background, or between isotropic voxels and background, were classified as boundary voxels. Isotropic diffusion voxels were considered to have equal diffusivity in all directions. Finally, The Orientation Distribution Function (ODF) in each voxel was estimated based on its class: background voxels were assigned zero ODF and the ODF in an isotropic voxel is considered as sphere. The ODFs of fibre bundle voxels and boundary voxels were reconstructed using Constrained Spherical Deconvolution (CSD) [7] with 6th and 2nd order spherical harmonics respectively. This was to account for crossing fibres in fibre bundle voxels and for one fibre bundle in boundary voxels.

III. Results and Discussion

The proposed sampling scheme, simulated noisy signal and its Fourier transform are illustrated in Figure 1. Note that low frequencies predominate in the signal. Figure 2 shows a slice before and after denoising.

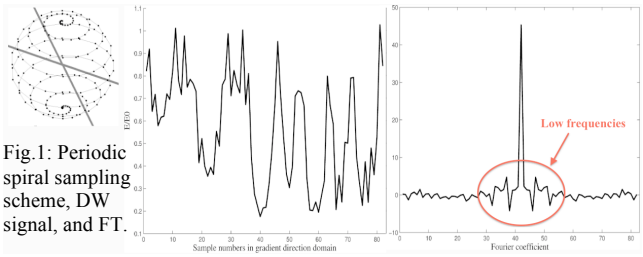

Fig.1: Periodic spiral sampling scheme, DW signal, and FT.

a 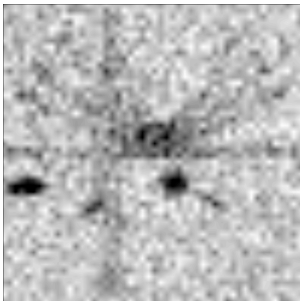 b 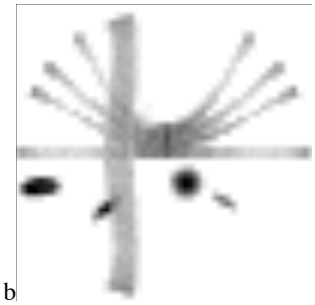

Fig. 2: a) A noisy slice of synthetic dataset 1 with SNR=10. b) Denoised slice (Background was determined using the proposed classification).

Figure 3 shows the decision three on the left and a representative slice classified on the right. Thresholds are learned from statistical analysis of the entire dataset.

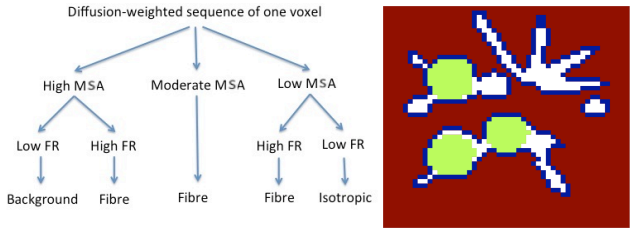

Fig. 3: Classification scheme (left) and an instance slice (right), where red denotes background, green isotropic diffusion, white fibres; and blue boundaries.

The proposed sampling scheme facilitated the identification of features of the diffusion-weighted signal, which allowed meaningful classification of image voxels. More sophisticated classification algorithms and a larger number of features (such as the number of extrema) can be used to improve classification results.

REFERENCES

[1] C. Pierpaoli, "Artifacts in diffusion MRI," in *Diffusion MRI; theory, methods and applications*, no. 18, D. K. Jones, Ed. New York: Oxford University Press, 2011, pp. 303–318.

[2] S. Pajevic, "Statistical issues in diffusion tensor MRI," in *Diffusion MRI; theory, methods and applications*, no. 20, D. K. Jones, Ed. New York: Oxford University Press, 2011, pp. 331–353.

[3] D. K. Jones, "Challenges and limitations of quantifying brain connectivity in vivo with diffusion MRI," *Imaging in Medicine*, vol. 2, no. 3, pp. 341–355, 2010.

[4] D. K. Jones, "The effect of gradient sampling schemes on measures derived from diffusion tensor MRI: A Monte Carlo study†," *Magn. Reson. Med.*, vol. 51, no. 4, pp. 807–815, 2004.

[5] J. P. Haldar, V. J. Wedeen, M. Nezamzadeh, G. Dai, M. W. Weiner, N. Schuff, and Z.-P. Liang, "Improved diffusion imaging through SNR-enhancing joint reconstruction," *Magn. Reson. Med.*, vol. 69, no. 1, pp. 277–289, Jan. 2013.

[6] J. D. Tournier, F. Calamante, and A. Connelly, "MRtrix: Diffusion tractography in crossing fiber regions," *Int. J. Imaging Syst. Technol.*, vol. 22, no. 1, pp. 53–66, 2012.

[7] J. D. Tournier, C. H. Yeh, F. Calamante, K. H. Cho, A. Connelly, and C.-P. Lin, "Resolving crossing fibres using constrained spherical deconvolution: Validation using diffusion-weighted imaging phantom data," *Neuroimage*, vol. 42, no. 2, pp. 617–625, Aug. 2008.